的补充信息
Supplementary Information for

闪光焦耳加热城市采矿
Urban Mining by Flash Joule Heating

Bing Deng1、Duy Xuan Luong1、Zhe Wang1、Carter Kittrell1、Emily A.McHugh1和James
Bing Deng[1], Duy Xuan Luong[1], Zhe Wang[1], Carter Kittrell[1], Emily A. McHugh[1], and James
M. 行程1,2,3,4*
M. Tour[1,2,3,4,*]

美国德克萨斯州休斯顿莱斯大学化学系，邮编77005
[1] Department of Chemistry, Rice University, Houston, Texas 77005, USA

美国得克萨斯州休斯顿莱斯大学斯莫利·考尔研究所，邮编：77005
[2] Smalley-Curl Institute, Rice University, Houston, Texas 77005, USA

美国德克萨斯州休斯顿莱斯大学纳米碳中心和韦尔奇先进材料研究所，邮编：77005
[3] NanoCarbon Center and the Welch Institute for Advanced Materials, Rice University, Houston, Texas 77005, USA

美国德克萨斯州休斯顿莱斯大学材料科学与纳米工程系，邮编：77005
[4] Department of Materials Science and NanoEngineering, Rice University, Houston, Texas 77005, USA

*通讯作者。 电子邮件：tour@rice.edu
*Corresponding author. Email: tour@rice.edu

补充说明

Supplementary Notes

补充说明1。 数值模拟。

Supplementary Note 1. The Numerical simulation.

使用有限元软件COMSOL Multiphysics 5.5进行了数值模拟。

The numerical simulation was conducted using the finite element software COMSOL Multiphysics 5.5.

温度模拟。

Temperature simulation.

对于温度分布模拟，使用交流/直流模块中的焦耳加热模式和以下参数(补充图6)：(1)几何参数：电极半径(0.4 cm)、电极长度(0.5 cm)、材料半径(0.4 cm)、材料长度(2 cm)。

For the temperature distribution simulation, the Joule Heating mode in the AC/DC module was used with the following parameters (**Supplementary Fig. 6**):

(1) geometrical parameters: electrode radius (0.4 cm), electrode length (0.5 cm), materials radius (0.4 cm), materials length (2 cm).

(2)材料参数：电导率(0.2 S m-1)和热导率(1 W m-1 K-1)。

(2) Materials parameters: electrical conductivity (0.2 S m^{-1}), and thermal conductivity (1 W m^{-1} K^{-1}).

(3)边界条件：输入电压(150 V)，接地(0 V)。

(3) Boundary conditions: input voltage (150 V), ground (0 V).

气体扩散模拟。

Gas diffusion simulation.

在典型的FJH工艺中，首先将容器泵送至P0～10 Pa。典型FJH后，压力为P1=12 kPa，因此收集的气体压力为P1=12 kPa。

In a typical FJH process, the vessel was first pumped to P_0 ~10 Pa. After a typical FJH, the pressure was P_1 = 12 kPa, hence the collected gas pressure was ΔP_1 = 12 kPa.

容器的体积为V1～40 mL，石英管的体积为V2～1 mL。

The volume of the vessel is V_1 ~40 mL, and the volume of the quartz tube is V_2 ~1 mL.

根据波义耳定律，方程式S1：

According to the Boyle's Law, **eq S1**:

$$V_1\Delta P_1 = V_2\Delta P_2 \quad \text{(S1)}$$

使用公式S2计算内部压力(P2)：

The inner pressure (ΔP_2) was calculated using **eq S2**:

$$\Delta P_2 = V_1\Delta P_1/V_2 = 480 \text{ kPa} \sim 5 \text{ atm}. \quad \text{(S2)}$$

因此，在FJH加热过程中产生的内部压力设定为5 atm，用于气体扩散模拟。

Hence, the inner pressure generated during the FJH heating was set as 5 atm for the gas diffusion simulation.

对于气体扩散模拟，层流模式用于以下方面
For the gas diffusion simulation, the Laminar Flow mode was used with the following 条件（补充图18）：
conditions (**Supplementary Fig. 18**):

（1）几何参数：反应器半径（0.4 cm）、反应器长度（2 cm）、管半径（0.1 cm）、管长度（4 cm）。
(1) Geometrical parameters: reactor radius (0.4 cm), reactor length (2 cm), tube radius (0.1 cm), tube length (4 cm).

（2）材料参数：温度（273.25 K）下的流体（N2）。
(2) Materials parameters: fluid (N_2) at temperature (273.25 K).

（3）边界条件：内压（500 kPa），外压（0 Pa，100 kPa，400 kPa）。
(3) Boundary conditions: inner pressure (500 kPa), outside pressure (0 Pa, 100 kPa, 400 kPa).

补充说明2。 回收率的计算

Supplementary Note 2. The calculation of recovery yield

对于蒸发分离，考虑到用于FJH的PCB原料质量为m(PCB)，PCB原料中的贵金属浓度测量为c(

For the evaporative separation, considering that the mass of PCB raw materials used

PCB)，冷阱中冷凝的贵金属质量为m(气体)，回收率(Y(气体))计算公式S3：

for FJH is *m*(PCB), the concentration of precious metals in PCB raw materials was measured as *c*(PCB), and the mass of precious metals condensed in the cold trap was *M*(Gas), the recovery yield (Y(Gas)) was calculated by as in **eq S3**:

$$Y(Gas) = \frac{M(Gas)}{c(PCB)\times m(PCB)} \times 100\% \qquad \text{(S3)}$$

或者，考虑到FJH后剩余固体(PCB闪蒸)的质量为m(PCB闪蒸)，贵金属的浓度为c(PCB闪蒸)，回

Alternatively, considering that the mass of remaining solid (PCB-Flash) after FJH was *m*(PCB-

收率也可以在等式S4中计算：

Flash), and the concentration of precious metals was *c*(PCB-Flash), the recovery yield could also be calculated in **eq S4**:

$$Y(Gas) = \frac{M(Gas)}{M(Gas)+c(PCB-Flash)\times m(PCB-Flash)} \times 100\% \qquad \text{(S4)}$$

在大多数情况下，这两种计算方法得出的结果相似，因为c(PCB)×m(PCB)=m(气体)+c(PCB闪

In most cases, the two-calculation methods gave similar results because *c*(PCB) × *m*(PCB) =

光)×m(PCB闪光)。 在这种情况下，使用了等式S1。 然而，在某些情况下，

M(Gas) + *c*(PCB-Flash) × *m*(PCB-Flash). In this case, **eq S1** was used. However, in some

由于贵金属在PCB原料中的分布不均匀，不同批次使用的PCB原料中贵金属的浓度有一定的差异。

cases, due to the inhomogeneous distribution of precious metals in PCB raw materials, the concentration of precious metals in the PCB raw materials used in different batches had some

这可能导致第一种方法的回收率>100%。 在这种情况下，方程

variation. This could result in a recovery yield >100% for the first method. In this case, **eq S2**

式S2用于给出较低的回收率限制。

was used to give a lower limitation of recovery yield.

为了提高FJH的浸出效率，考虑到FJH使用的PCB原料质量为m(PCB)，PCB原料中的贵金属浓度测

For the FJH-improved leaching efficiency, considering that the mass of PCB raw

量为c(PCB)，PCB闪蒸固体质量为m(PCB闪蒸)，PCB闪蒸固体中的贵金属浓度测量为c(PCB闪蒸)

materials used for FJH was *m*(PCB), the concentration of precious metals in PCB raw materials

，然后通过浸出PCB闪蒸固体获得回收率，Y(PCB闪光)，使用公式S5计算：

was measured as *c*(PCB), the mass of PCB-Flash solid was *m*(PCB-Flash), the concentration of precious metals in PCB-Flash solid was measured as *c*(PCB-Flash), then the recovery yield by leaching the PCB-Flash solid, Y(PCB-Flash), was calculated using **eq S5**:

$$Y(PCB-Flash) = \frac{c(PCB-Flash)\times m(PCB-Flash)}{c(PCB)\times m(PCB)} \times 100\% \qquad \text{(S5)}$$

类似地，通过浸出PCB煅烧的回收率Y(PCB煅烧)使用公式S6计算：

Similarly, the recovery yield by leaching the PCB-Calcination, Y(PCB-Calcination), was calculated using **eq S6**:

$$Y(PCB-Calcination)=\frac{c(PCB-Calcination)\times m(PCB-Calcination)}{c(PCB)\times m(PCB)}\times 100\% \quad (S6)$$

其中，m(PCB煅烧)是PCB煅烧固体的质量，c(PCB闪蒸)是PCB煅烧固体中贵金属的浓度。

where *m*(PCB-Calcination) was the mass of PCB-Calcination solid, the *c*(PCB-Flash) was the concentration of precious metals in PCB-Calcination solid.

使用公式S7计算PCB闪速煅烧浸出回收率Y(PCB闪速煅烧)：

The recovery yield by leaching the PCB-Flash-Calcination, Y(PCB-Flash-Calcination), was calculated using **eq S7**:

$$Y(PCB-Flash-Calcination)=\frac{c(PCB-Flash-Calcination)\times m(PCB-Flash-Calcination)}{c(PCB)\times m(PCB)}\times 100\% \quad (S7)$$

100%(S7)，其中m(PCB闪速煅烧)是PCB煅烧固体的质量，c(PCB闪速煅烧)是PCB煅烧固体中贵金属的浓度。

where *m*(PCB-Flash-Calcination) was the mass of PCB-Calcination solid, the *c*(PCB-Flash-Calcination) was the concentration of precious metals in PCB-Calcination solid.

对于FJH去除有毒重金属，考虑到FJH所用PCB原料的质量为m(PCB)，PCB原料中重金属的浓度测量为c(PCB)，PCB闪蒸固体的质量为m(PCB闪蒸)，PCB闪蒸固体中贵金属的浓度测量为c(PCB闪蒸)，然后去除效率，Y(去除)，使用公式S8计算FJH产生的有毒重金属含量：

For the removal of toxic heavy metals by FJH, considering that the mass of PCB raw materials used for FJH was *m*(PCB), the concentration of heavy metals in PCB raw materials was measured as *c*(PCB), the mass of PCB-Flash solid was *m*(PCB-Flash), the concentration of precious metals in PCB-Flash solid was measured as *c*(PCB-Flash), then the removal efficiency, Y(Removal), of toxic heavy metals by FJH was calculated using **eq S8**:

$$Y(Removal)=\frac{c(PCB)\times m(PCB)-c(PCB-Flash)\times m(PCB-Flash)}{c(PCB)\times m(PCB)}\times 100\% \quad (S8)$$

此外，考虑到通过冷凝在冷阱中收集的有毒重金属质量为M(气体)，收集量Y(收集量)使用公式S9计算：

Furthermore, considering that the mass of toxic heavy metals collected by condensation in the cold trap was *M*(Gas), the collection yield, Y(Collection), was calculated using **eq S9**:

$$Y(Collection)=\frac{c(PCB-Flash)\times m(PCB-Flash)}{c(PCB)\times m(PCB)}\times 100\% \quad (S9)$$

补充说明3。 收集固体的总成分分析以及基于证据的纯化和精炼预测。

Supplementary Note 3. The total composition analysis of the collected solid and evidence-based predictions on purification and refining.

蒸发分离收集的固体是金属混合物。 已经有许多商业流程可以将单个金属从金属混合物中分离出来。

The collected solids by the evaporative separation are a mixture of metals. There are already many commercial processes to separate individual metals from a mixture of metals. 在这里，我们首先对收集的固体中的金属(类型和含量)进行了完整的成分调查，并提供了基于证据的预测，说明如何使用易于获取、成熟的方法分离单个金属。

Here, we first did a complete composition investigation of metals (type and content) in the collected solids and provide evidence-based predictions on how to separate individual metals using readily accessible, well-established methods.

收集固体的总成分分析。

The total composition analysis of the collected solid.

我们使用不含化学添加剂的收集固体，以及含有混合卤化物添加剂(NaF、NaCl和NaI)的收集固体作为代表。 测定了电子废物中的丰富金属(铜、锡、铝、铁和锌)、贵金属(铑、钯、铂、银和金)和有毒重金属(汞、镉、砷、铅和铬)。

We use the collected solid without chemical additive, and the collected solid with mixture halide additives (NaF, NaCl, and NaI) as representatives. The abundant metals in e-waste (Cu, Sn, Al, Fe, and Zn), the precious metals (Rh, Pd, Pt, Ag, and Au), and the toxic heavy metals (Hg, Cd, As, Pb, and Cr) were measured. 由于其他金属的含量比丰富金属的含量少几个数量级，我们认为考虑上述元素可以提供合理的近似值。

Since the content of other metals are a few orders of magnitude less than those of the abundant metals, we think that the consideration of the above elements affords a reasonable approximation. 收集的固体被完全消化，并对金属进行ICP-MS分析。

The collected solid was totally digested and the ICP MS analysis of the metals was conducted. 添加和不添加添加剂的收集固体的总金属成分如补充图14所示。 在这两种情况下，最丰富的成分是大于60 wt%的Cu，其次是大于1 wt%的Al、Sn、Fe和Zn。

The total metal composition of the collected solids with and without the additives was shown in **Supplementary Fig. 14**. In both cases, the most abundant components are Cu with >60 wt%, followed by Al, Sn, Fe, and Zn with >1 wt%. 对于贵金属，质量比为Ag，约0.6 wt%；Pd，约0.04 wt%；相对湿度，约0.02 wt%；和Au，约0.01 wt%。铜是一种主要的可回收金属，约占城市采矿总价值的30%，因此我们的FJH工艺也适用于从电子废物中回收铜。

For precious metals, the mass ratios were Ag, ~0.6 wt%; Pd, ~0.04 wt%; Rh, ~0.02 wt%; and Au, ~0.01 wt%. Cu is one major metal to be recovered with ~30% of total values for urban mining, so our FJH process also works for Cu recovery from e-waste.

收集的固体中贵金属的化学状态。

The chemical states of precious metals in the collected solid.

由于贵金属含量<0.1 wt%(补充图14)，很难直接进行XPS分析。

Since the content of precious metals are <0.1 wt% (Supplementary Fig. 14), it is difficult to directly conduct the XPS analysis. 在这里，我们将贵金属盐添加到e-

废物，并进行相同的FJH程序，以收集挥发物进行XPS分析。
waste and conducted the same FJH procedure to collect the volatiles for the XPS analysis. 具体而言，将RhCl3、PdCl2、AgCl和HAuCl4添加到电子废物和炭黑(CB)的混合物中，每种重量比为5
Specifically, $RhCl_3$, $PdCl_2$, AgCl, and $HAuCl_4$ were added into the mixture of e-waste and wt%。 在相同的FJH工艺之后，收集挥发物并
carbon black (CB) with a weight ratio of 5 wt% for each. After the same FJH process, the 进行XPS测量以分析贵金属的化学状态。
volatiles were collected and XPS measurements were conducted to analyze the chemical states 如补充图16所示，Ag和Au主要处于元素状态。
of the precious metals. As shown in Supplementary Fig. 16, the Ag and Au were mainly in the Au 4f7/2在85.2 eV处的副峰可能来自Au基金属合金，例如AuIn2。
elemental state. The minor peak at 85.2 eV for Au $4f_{7/2}$ could be from an Au-based metal alloy, Rh和Pd均存在元素态和氧化态。 310.4 eV处的
for example, $AuIn_2$. For Rh and Pd, both elemental and oxidation states existed. The Rh $3d_{5/2}$ Rh 3d5/2峰可分配给RhCl3，338.0 eV处的Pd 3d5/2峰可分配给PdCl2。
peak at 310.4 eV could be assigned to $RhCl_3$, and the Pd $3d_{5/2}$ peak at 338.0 eV could be 这种差异可能归因于贵金属的不同化学反应性。
assigned to $PdCl_2$. This difference might be attributed to the different chemical reactivity of the precious metals.

贵金属提纯和精炼的循证预测。
Evidence-based prediction on the purification and refining of precious metals.

个别贵金属的分离和精炼已有一些商业流程，包括选择性沉淀、溶剂萃取和固相萃取1,2。
There have been a few commercial processes for individual precious metals separation and refining, including selective precipitation, solvent extraction and solid-phase extraction[1,2]. 经典的沉淀方法是基于贵金属氯络合物3铵盐的溶解度差异。
The classical precipitation methods are based on the solubility difference of the ammonium salts of precious metal-chloro complexes[3]. 溶剂萃取法使用溶剂萃取剂选择性萃取给定金属，然后
The solvent extraction methods use solvent extractants to selectively extract a given metal and then transfer to the organic phase[4]. 转移到有机相4。 固相萃取依赖于使用具有金属选择性配体的离子交换树脂5。
The solid-phase extraction relies on the use of ion-exchange resins with metal-selective ligands[5]. 所有这些成熟的技术都可以直接用于我们收集的固体中，以纯化和精炼单个贵金属。
All these well-established techniques could be directly used in our collected solid for purification and refinement of individual precious metals.

补充说明4。蒸发分离过程的分离能力。

Supplementary Note 4. Separation capability of the evaporative separation process.

从复杂的电子废物中获得易于使用的纯金属通常需要一个漫长的工程包，包括从选矿到净化。它通常有两个主要过程，即从电子废物原料中回收金属混合物，以及随后从混合物中分离或精炼单个金属。在商业实践中，在对电子废物进行检查和选矿后，采用火法冶金工艺(熔炼)获得金属混合物固体。然后采用湿法冶金工艺(浸出)获得含混合金属的浸出液。最后，采用先进的精炼工艺分离和提纯单个金属，主要技术包括溶剂萃取、浸出沉淀、电氧化和离子交换2。

Obtaining readily applicable pure metals from the complex e-waste usually relies on a lengthy engineering package, including beneficiation to purification. It usually has two major processes, the recovery of metal mixture from the e-waste raw materials, and the subsequent separation or refining of individual metals from the mixture. In commercial practices, after examination and beneficiation of the e-waste, the pyrometallurgical process (smelting) is applied to obtain a mixture solid of metals. Then the hydrometallurgical process (leaching) is used to obtain the leaching liquor with mixed metals. Finally, advanced refining process are used to separate and purify individual metals, with the main techniques including solvent extraction, leaching-precipitation, electro-oxidation and ion exchange[2].

在手稿中，我们提出的蒸发分离首先是针对电子废物基质(如塑料、陶瓷和碳)中的金属分离。如此高的温度(约3000 K)，加上添加剂的辅助，可以蒸发大部分金属。我们并不寻求获得纯净的单个金属。蒸发分离方案具有分离金属的能力，可通过进一步优化FJH装置来改进。本文首先讨论了基于蒸汽压差的金属理论分离因子以及合金熔体形成对分离因子的影响；其次，我们讨论了目前实现的分离能力；第三，讨论了化学添加剂辅助分离；第四，我们对如何进一步改进蒸发分离方案的分离进行了基于证据的预测。

In the manuscript, our proposed evaporative separation is first-of-all targeted on the separation of metals from the matrices (such as plastic, ceramics and carbon,) of e-waste. Such a high temperature (~3000 K), and assisted by the additives, could evaporate most of the metals. We did not seek to obtain the pure, individual metals. The evaporative separation scheme exhibits a capability for the separation of metals, which could be improved by further optimization of the FJH setup. We here first discuss the theoretical separation factor of metals based on the vapor pressure difference and the effect of alloy melt formation on the separation factors; second, we discuss the separation ability achieved now; third, we discuss the chemical additives assisted separation; fourth, we made evidence-based predictions regarding how to further improve the separation of the evaporative separation scheme.

基于蒸汽压差的蒸发分离过程的理论分离因子。

Theoretical separation factors of the evaporative separation process based on the vapor pressure difference.

电子废物含有元素周期表中的大部分金属。在这里，我们选择了电子垃圾中丰富的金属：铜、锡、铝、铁和锌；贵金属Rh、Pd、Pt、Ag和

The e-waste contains most of the metals across the Periodic Table. Here, we choose the abundant metals in e-waste: Cu, Sn, Al, Fe, and Zn; the precious metals Rh, Pd, Pt, Ag, and

Au；并以有毒重金属Hg、Cd、As、Pb、Cr为代表，计算其分离因子。
Au; and the toxic heavy metals Hg, Cd, As, Pb, and Cr, as representatives to calculate their

补充图21a中绘制了这些金属和C的蒸气压-温度关系图。
separation factors. The vapor pressure-temperature relationships of these metals and C are

如果我们不考虑合金对蒸汽压的影响，这些金属的理论分离系数可
plotted in **Supplementary Fig. 21a**. If we do not consider the alloy effect on the vapor pressure,

以根据蒸汽压差通过方程式S10计算得出，
the theoretical separation factors of these metals could be calculated based on the vapor

pressure differences by **eq S10**,

$$\beta_{A-B} = \frac{P_A(t=t_{b,A})}{P_B(t=t_{b,A})} \qquad \text{(S10)}$$

式中，A-B是金属A和金属B的分离系数，PA(t=tb，A)是
where $\beta_{A\text{-}B}$ is the separation factor of metal A and metal B, $P_A(t = t_{b,A})$ is the vapor pressure of

金属A的沸点为金属A(tb，A)，PB(t=tb，A)是金属B在tb，A的蒸气压。
metal A at the boiling point of metal A ($t_{b,A}$), and $P_B(t = t_{b,A})$ is the vapor pressure of metal B

分离系数列在补充表3中，并绘制在
at $t_{b,A}$. The separation factors are listed in **Supplementary Table 3** and plotted in

补充图21b。
Supplementary Fig. 21b.

在大多数情况下，蒸发分离的分离系数大于100，表明蒸发分离是一种潜在的金属分离过程。
In most cases, the evaporative separation has a large separation factor of >100,

热图
demonstrating that the evaporative separation is a potential process for metal separation. The

显示，金属可分为几个簇，低沸点组：Hg、As、Cd、Zn和Pb；中沸点组：Ag、Al、Cu、Sn、Cr、Au、Fe和Pd
heatmap shows that the metals could be grouped into a few clusters, the group with low boiling

；高沸点组：Rh和Pt。
points: Hg, As, Cd, Zn, and Pb; the group with median boiling points: Ag, Al, Cu, Sn, Cr, Au,

重金属往往沸点较低，最容易从电子
Fe, and Pd; and the group with high boiling points: Rh and Pt. The heavy metals tend to have

垃圾中去除，其次是丰富的金属基团，然后是贵金属基团。
low boiling points and are the easiest to be removed from the e-waste, followed by the abundant

对于蒸气压差较大的元素，分离因子较大，如flAg
metal groups, and then the precious metal groups. For the elements with large vapor pressure

Pd～2439；相比之下，对于具有类似蒸发行为的金属，例如Cu-Al ~ 1.25，分离因子较小。
difference, the separation factor is large, *e.g.*, $\beta_{Ag\text{-}Pd}$ ~ 2439; in contrast, the separation factor is

small for the metals with similar evaporative behavior, *e.g.*, $\beta_{Cu\text{-}Al}$ ~ 1.25.

熔体合金形成对分离因子的影响。
The effect of melt alloy formation on the separation factors.

FJH过程中可能会形成合金，但这不是必然的。 在电子废物中
There might be alloy formation during the FJH process, yet it is not a certainty. In e-waste,

，金属通常由基体基底分离，在FJH过程中加热速度超快(>104 K s-1)，反应时间短(~1s)。
the metals are usually separated by the matrix substrates, and the heating rate is ultrafast (>10^4

因此，金属在升华之前可能不会形成
K s^{-1}) in the FJH process with short reaction duration (~1 s). As a result, the metals might not

合金。 此外，并非所有金属都会形成固溶体。
form alloys before their sublimation. Moreover, not all the metals will form a solid solution.

例如，Ag和Cu在热力学上是不互溶的，因此熔化对其蒸发行为没有影响。
For example, Ag and Cu are thermodynamically immiscible, hence the melting will have no effect on their evaporative behaviors.

在合金熔体形成的情况下，我们讨论了合金上各金属组分的分蒸气压。
In the case of alloy melt formation, we discuss the partial vapor pressure of each metal components over alloys. 为了简单起见，我们考虑二元合金AB。 For simplicity purposes, we consider the binary alloys AB. 液态合金上的平衡分蒸气压由方程式S11给出：6=6 8 6(S11)，其中pA是金属A的分蒸气压，6 8是纯金属A的蒸气压，aA是合金AB中组分A的活性。
The equilibrium partial vapor pressure over liquid alloys is given by **eq S11**:

$$p_A = p_A^0 a_A \qquad \text{(S11)}$$

where p_A is the partial vapor pressure of metal A, p_A^0 is the vapor pressure of pure metal A, and a_A is the activity of component A in the alloy AB.

该活性具有以下性质：(1)对于不显示固溶体的纯相，a=1。
The activity has the following properties: (1) $a = 1$ for a pure phase that does not exhibit solid solution. 因此，对于不形成合金的金属，如铜和银，熔化对其蒸气压没有影响。 Hence, for the metals that do not form alloys, like the case of Cu and Ag, the melting has no effect on their vapor pressure. (2)活性与摩尔分数(x)有关。 (2) The activity is related to the mole fraction (x). 在理想模型中，活度等于摩尔分数，6=6。 In an ideal model, the activity equals to the mole fraction, $a_A = x_A$. 在非理想模型中，根据正常活性组成图(补充图22)，一种组分在极低摩尔分数或极高摩尔分数下表现出近乎理想的行为。 In a non-ideal model, according to the normal activity-composition diagram (**Supplementary Fig. 22**), one component exhibits nearly ideal behavior at very low mole fractions or very high mole fractions. 对于此类组合物，活性约等于摩尔分数。 For such compositions, activity is approximately equal to mole fraction. 在我们的案例中，贵金属和重金属是痕量金属(约10 ppm水平)，而主要金属，如铜、锡和铝，则>1 wt%(>10000 ppm水平)(补充图14)。 In our cases, the precious metals and heavy metals are trace metals (~10 ppm level), and the major metals, such as Cu, Sn, and Al, are >1 wt% (>10000 ppm level) (**Supplementary Fig. 14**). 因此，活性几乎等于贵金属和重金属的摩尔分数。 Hence, the activity nearly equals the mole fraction for precious metals and heavy metals. 换句话说，固体熔体的形成不会对其蒸发行为产生明显影响。 In other words, the formation of solid melt will not have an apparent effect on their evaporative behavior. Ag、Pd、Au、Rh、Pt、Cr、As、Pb、Hg和Cd的计算分离系数通常不受含有大量金属(包括Cu、Sn、Al、Fe和Zn)的合金熔体形成的影响(补充表3)。 The calculated separation factors for Ag, Pd, Au, Rh, Pt, Cr, As, Pb, Hg, and Cd are generally not affected by the formation of alloy melt with abundant metals including Cu, Sn, Al, Fe, and Zn (**Supplementary Table 3**). (3)活性由合金中A的化学势决定。 (3) The activity is determined by the chemical potential of A in the alloy. 对于具有可比成分水平的组分，活性将偏离摩尔分数。 For the components at comparable composition level, the activity would deviate from the mole fraction. 在这些情况下，应根据活动校正分离系数。 In these cases, the separation factors should be corrected based on the activity. 例如，铜和铝是电子废物中的丰富金属。 For example, Cu and Al are abundant metals in e-waste. 有文献报道 There is literature reporting

液态Cu-Al合金中各组分的活性6。 铜和铝的分离系数应进行相应的修正。
the activity of the constituents in liquid Cu-Al alloy[6]. The separation factor of Cu and Al should

在我们目前的工作中，我们的目标是分离贵金属和重金属(如痕量金属)，
be corrected accordingly. In our present work, we are targeting the separation of precious

因此我们不寻求计算丰富金属的精确分离系数。
metals and heavy metals (as trace metals), hence we do not seek to calculate the precise

separation factor for the abundant metals.

通过蒸发分离实现的分离能力。
The achieved separation ability by the evaporative separation.

如图1g所示，在没有化学添加剂的情况下，贵金属的回收率为Y(Rh)=4.0%，Y(Pd)=3.1%，Y(
As shown in **Fig. 1g**, without the chemical additives, the recovery yields for the precious

Ag)=38.0%，Y(Au)=1.3%。 这些不同的回收率
metals were Y(Rh) = 4.0%, Y(Pd) = 3.1%, Y(Ag) = 38.0%, and Y(Au) = 1.3%. These different

值证明了FJH工艺的分离能力(补充表4)。
recovery yield values demonstrate the separation ability of the FJH process (**Supplementary**

例如，Au和Ag的分离因子为flAg Au ~ 29.2。 该值与flAg Au
Table 4). For example, the separation factor of Au and Ag is $\beta_{\text{Ag-Au}}$ ~ 29.2. This value is

的理论计算分离因子理论值35相当
comparable with the theoretical calculated separation factor of $\beta_{\text{Ag-Au, theory}}$ ~ 35

(补充表3)。
(**Supplementary Table 3**).

从化学添加剂中分离金属的能力。
The metal separation ability from the chemical additives.

在这篇手稿中，我们展示了使用卤化物添加剂提高贵金属回收率(图。
In this manuscript, we demonstrate an improved recovery yield of precious metals by using

卤化物的类型也会影响分离因子。
the halide additives (**Figs. 2a-f**). The type of halide also affects the separation factors.

例如，通过使用NaCl作为添加剂，我们实现了Y(Rh)=25.2%、Y(Pd)=17.5%、Y(Ag)=75.8%
For example, by using NaCl as the additive, we achieved recovery yield of Y(Rh) = 25.2%,

和Y(Au)=0.3%的回收率。因此，计算分离系数(补充表5)。
Y(Pd) = 17.5%, Y(Ag) = 75.8%, and Y(Au) = 0.3%. Accordingly, the separation factors are

同样，通过使用NaF作为添加剂，我们实现了Y(Rh)=87.7%
calculated (**Supplementary Table 5**). Similarly, by using NaF as the additive, we achieved

、Y(Pd)=57.8%、Y(Ag)=48.6%和Y(Au)=0.6%的回收率。 以
recovery yield of Y(Rh) = 87.7%, Y(Pd) = 57.8%, Y(Ag) = 48.6%, and Y(Au) = 0.6%. By

NaI为添加剂，回收率分别为Y(Rh)=39.6%，Y(Pd)=41.7%，Y(Ag)=42.7%，Y(Au)=63%。
using NaI as additive, we achieved recovery yield of Y(Rh) = 39.6%, Y(Pd) = 41.7%, Y(Ag)

计算了使用NaF和NaI作为添加剂的分离因子(补充表6-7)。
= 42.7%, and Y(Au) = 63%. The separation factors by using NaF and NaI as the additives were

结果表明，Cl对Ag最为有效，F对Rh和Pd最为有效，I对Au最
calculated (**Supplementary Tables 6-7**). It is found that Cl works best for Ag, F works best

为有效。
for Rh and Pd, and I work best for Au.

因此，使用卤化物作为添加剂可以提高回收率，同时改变分离因子。
Hence, the use of halides as additives could improve the recovery yield, while at the same time change the separation factors. 通过引入添加剂进行金属分离归因于贵金属与化学添加剂的不同化学反应性，可以进一步优化以获得更好的分离能力。The metal separation by the introduction of additives is attributed to the different chemical reactivity of precious metals with the chemical additives, which could be presumably further optimized for a better separation ability. 例如，在未来的研究中，我们可以首先添加含Cl的添加剂来分离Ag，然后添加含F的添加剂来分离Rh和Pd，然后添加含I的添加剂来分离Au。For example, in future studies, we can first add Cl-containing additives to separate Ag, then F-containing additives to separate Rh and Pd, and then I-containing additives to separate Au. 回收率和分离能力之间存在权衡；在这篇手稿中，我们关注的是高回收率，并没有寻求高分离能力。There is a tradeoff between recovery yield and separation ability; we focused on a high recovery yield in this manuscript and did not seek high separation ability.

以证据为基础的预测实践，以增加分离系数。
The evidence-based predictions on the practices to increase the separation factors.

我们注意到，实现的分离系数低于理论计算值(补充表3-7)。
We noticed that the achieved separation factors are lower than the theoretically calculated ones (**Supplementary Tables 3-7**). 为了进一步提高分离能力，我们认为更仔细地控制温度和反应时间将是有益的，这是蒸发分离方案的下一步。To further increase the separation ability, we think that more carefully controlled temperatures and reaction duration would be helpful, which is the next step for the evaporative separation scheme. 我们目前正在升级FJH系统，使其具有更好的温度可控性。We are currently upgrading our FJH system with better temperature controllability. 在未来，我们假设通过逐步提高FJH温度来逐个蒸发金属。In the future, we presume to evaporate the metals one-by-one by progressively increasing the FJH temperature. 我们再次注意到，回收率和分离能力之间总是存在权衡。We again note that there is always tradeoff between recovery yield and separation ability. 我们目前的工作主要集中在高回收率上，因此在分离方面投入较少。Our current work mainly focused on the high recovery yield and hence put less effort toward the separation. 进一步的工作对于平衡回收率和金属分离至关重要。Further work is essential to balance the recovery yield and metal separation.

补充说明5。 能源消耗与成本评估

Supplementary Note 5. The energy consumption and cost evaluation

使用方程式S12计算能耗：

The energy consumption was calculated using **eq S12**:

$$E = \frac{(V_1^2 - V_2^2) \times C}{2 \times M} \quad \text{(S12)}$$

其中E是每克能量(kJ g-1)，V1和V2分别是闪光焦耳加热前后的电压，C是电容(C=60 mF)，M是每

Where E is the energy per gram (kJ g^{-1}), V_1 and V_2 are the voltage before and after flash Joule

批的质量。

heating, respectively, C is the capacitance (C = 60 mF), and M is the mass per batch.

对于典型试验，V1=150 V，V2=0 V，M=0.2 g，能量计算为：

For a typical trial, V_1 = 150 V, V_2 = 0 V, and M = 0.2 g, the energy was calculated to be:

E=3.38 kJ g-1=9.39×10-4 kWh g-1=939 kWh吨-1

E = 3.38 kJ g^{-1} = 9.39 × 10^{-4} kWh g^{-1} = 939 kWh ton^{-1}

考虑到美国德克萨斯州的工业电能价格为0.02 kWh-1美元，处理1吨电子垃圾的成本为P=18.78吨-1美元。

Given that the industrial price of electric energy in Texas, USA is \$0.02 kWh^{-1}, the cost for

treatment of 1 ton of e-waste would be P = \$18.78 ton^{-1}.

作为实验室规模的参考，Balaji等人对使用管状炉7使用火法冶金从PCB中回收金属进行了成本效益分析

As a reference at the laboratory scale, Balaji *et al.* conducted a cost-benefit analysis on

。 对于质量为200 g的PCB

metal recovery from PCB using pyrometallurgy using a tubular furnace[7]. For the PCB mass of

，他们报告的耗电量为100 kWh。 这相当于5×105 kWh吨-1，或104美元

200 g, they reported the electrical consumption of 100 kWh. This corresponds to 5 × 10^5 kWh

吨-1。 FJH工艺的成本为939 kWh t-1或18.78美元t-1，相当于管式炉的约1/500。

ton^{-1}, or \$$10^4$ ton^{-1}. The cost of the FJH process is 939 kWh ton^{-1} or \$18.78 ton^{-1}, corresponding

在一个工业规模的案例中，Boliden有限公司。 瑞典龙斯卡

to ~1/500 of that of the tubular furnace. In an industrial-scale case, Boliden Ltd. Ronnskar

冶炼厂使用卡尔多炉进行冶炼8。 电子废物通过卡尔多炉转化为混合铜合金，这

Smelter, Sweden used a Kaldo furnace for smelting[8]. The e-waste was converted into a mixed

与我们使用FJH装置通过蒸发分离收集的固体类似。

Cu alloy by the Kaldo furnace, which is similar to our collected solids by evaporative separation

他们报告了电子废物处理所需的274 GJ吨-1能量。

using the FJH setup. They reported the required energy of 274 GJ ton^{-1} for e-waste processing.

而在我们的情况下，能耗为3.38 GJ吨-1，相当于卡尔多炉的约1/80。

While in our case, the energy consumption is 3.38 GJ ton^{-1}, corresponding to ~1/80 of the

我们注意到，商业卡尔多炉的能耗已得到优化，我们认为，当规模扩大到工业规模时，我

Kaldo furnace. We note that the energy consumption is optimized for the commercial Kaldo

们FJH装置的能耗可能会进一步降低。

furnace, and we presume the energy consumption of our FJH setup could be further reduced

when scaling up to industrial scale.

补充说明6。FJH工艺放大策略。

Supplementary Note 6. Strategy for scaling up of the FJH process.

焦耳加热是一种成熟的加热技术，已广泛应用于多个实际设备和工业过程，例如电保险丝和电加热器。这里公开的FJH本质上是焦耳加热过程。FJH与传统焦耳加热技术的区别在于电能供应方式和加热持续时间。传统的焦耳加热过程使用直流(DC)或交流(AC)电源来提供稳定的电输出。对于我们的FJH工艺，使用电容器组在短时间内(低至毫秒级)提供脉冲电压输出。FJH流程确实具有高度可扩展性。本文首先对FJH过程的标度规律进行了理论分析；其次，我们提到了在我们的研究实验室进行的批量放大实验，生产能力达到kg级；第三，我们对FJH过程如何通过连续的滚动方式进行扩展进行了基于证据的预测；第四，我们简要讨论了FJH工艺正在进行的工业规模应用。

Joule heating is a mature heating technique and has been widely used in multiple practical devices and industrial processes, for example, electric fuses and electric heaters. The FJH disclosed here is intrinsically a Joule heating process. The difference of the FJH and conventional Joule heating technique lies in the modes of electrical energy supply and the heating duration. The conventional Joule heating process uses direct current (DC) or alternating current (AC) sources to provide a stable electric output. For our FJH process, a capacitor bank is used to provide a pulsed voltage output in a short time (down to ms scale). The FJH process is indeed highly scalable. Here, we first conduct the theoretical analysis on the scaling rule of the FJH process; second, we mention the batch-by-batch scaling up experiments with productivity up to kg scale in our research lab; third, we make an evidence-based prediction on how the FJH process could be scaled up by a continuous, roll-to-roll manner; fourth, we briefly discuss the undergoing industrial-scale application of the FJH process.

通过理论分析揭示了FJH过程的标度规律。

The scaling rule of FJH process revealed by theoretical analysis.

可接近的高温和整个区域的均匀温度分布

The *accessible high temperature* and the *uniform temperature distribution* across the sample are the two key points when scaling up the FJH process. For Joule heating, the heat amount (Q) is determined by **eq S13**,

等式S13确定，=：(S13)，其中I是通过样品的电流，R是样品的电阻，t是放电时间。

$$Q = I^2Rt \qquad \text{(S13)}$$

where I is the current passing through the sample, R is the resistance of the sample, and t is the discharging time. 然后，我们考虑由等式S14确定的单位体积热量(Qv)，；=：<(S14) We then consider the heat per volume (Q_v) determined by **eq S14**,

其中j是电流密度，e是电阻率，t是放电时间。

$$Q_v = j^2\rho_e t \qquad \text{(S14)}$$

where j is the current density, ρ_e is the electrical resistivity, and t is the discharging time.

温度与热量成正比，因为样品的热容是恒定的。
The temperature is proportional to the heat since the heat capacity of the sample is constant.
由于样品的电阻率是恒定的，为了在放大样品时保持恒定的Qv和t，我们需要保持恒定的j。
Since the electrical resistivity of the sample is constant, to maintain a constant Q_v and t when scaling up the sample, we need to maintain a constant j.

电容器组中的电荷(q)由等式S15确定，
The charge (q) in the capacitor bank is determined by **eq S15**,

=(S15)，其中C是总电容，V是充电电压。

$$q = CV \tag{S15}$$

如果我们假设电容器组中的电荷在
where C is the total capacitance, and V is the charging voltage. If we suppose the charges in
放电时间t内放电，则通过公式S16计算通过样品的电流(I)，
the capacitor bank are discharged in the discharging time of t, the current (I) passing through the sample is calculated by **eq S16**,

$$I = \frac{q}{t} \tag{S16}$$

然后，通过等式S17确定电流密度(j)，
Then, the current density (j) is determined by **eq S17**,

$$j = \frac{I}{S} = \frac{CV}{St} \tag{S17}$$

其中S是样品的横截面积。 考虑到圆柱形样品(通常情况下)，样品质量
where S is the cross-sectional area of the sample. Considering the cylinder-shaped sample
(m)通过公式S18计算，
(which is usually the case), the sample mass (m) is calculated by **eq S18**,

=，(S18)其中，m是样品的密度，S是样品的横截面积，L是样品的长度
。

$$m = \rho_m SL \tag{S18}$$

where ρ_m is the density of the sample, S is the cross-sectional area of the sample, and L is the length of the sample.

最重要的是，我们得到了确定等式S19电流密度的公式，
Above all, we obtain a formula determining the current density of **eq S19**,

$$j = \frac{CV\rho_m L}{mt} \tag{S19}$$

如前所述，为了扩大样品质量(m)，我们需要保持恒定的电流密度。
As discussed, to scale up the sample mass (m), we need to maintain a constant current density.
这可以通过以下措施实现：(1)增加FJH电压(V)，和/或(2)增加电容(C)。
This could be realized by the measures of (1) increasing the FJH voltage (V), and/or (2) increasing the capacitance (C).

在FJH装置中，我们使用商用铝电解电容器(450 V，6 mF，Mouser#80-PEH200YX460BQU2)。
In our FJH setup, we use a commercial aluminum electrolytic capacitor (450 V, 6 mF, Mouser #80-PEH200YX460BQU2). 最先进的商用铝电解电容器的最大额定电压为V1=630 V，电容为C1=2.7 F。 在我们的
The state-of-art commercial aluminum electrolytic capacitor has the maximum rated voltage of V_1 = 630 V, and capacitance of C_1 = 2.7 F. In our

典型实验中，对于质量为m0=0.2 g的样品，我们使用V0=150 V的FJH电压和C0=0.06 F的FJH。根据方程式
typical experiment, we use a FJH voltage of V_0 = 150 V and C_0 = 0.06 F for the FJH of sample
S18，仅使用一个最先进的电容器，每批质量为m1=m0(C1 V1)/(C0V0)=37.8 g。
with mass of m_0 = 0.2 g. According to eq S18, by using just one state-of-art capacitor, the mass
电容器可以并联，通过等式S20，454$0=B+：+++3(S20
is $m_1 = m_0 (C_1 V_1)/(C_0V_0)$ = 37.8 g per batch. The capacitors could be connected in parallel to
)获得高总电容
get a high total capacitance by **eq S20**,

$$C_{total} = C_1 + C_2 + \cdots + C_n \qquad \text{(S20)}$$

考虑到我们使用的电容器组由30个铝电容器组成，总电容为Ctotal=81 F，在1s的放电时间内，每批的质量
Considering that we use a capacitance bank composed of 30 aluminum capacitors with
为mbatch=1.1 kg。
the total capacitance of C_{total} = 81 F, the mass will be m_{batch} = 1.1 kg per batch in the discharging
电容器组的重新充电是该过程中最慢的步骤，可以通过高速充电技术进行补偿。
time of 1 s. The re-charging of the capacitor bank is the slowest step of the process, which
假设总时间为ttotal=每批10秒，一个
could be compensated by a high-speed charging technique. Supposing the total time is t_{total} =
这样的FJH装置可以每天处理约10吨的电子废物。根据我们的
10 s per batch, one such FJH setup could process the e-waste of m ~ 10 tons per day. Based on
经验和这些计算，可以合理地得出以下结论：FJH工艺具有高度的可扩展性，具有工业规模应用的能力。
our experience and these calculations, it is reasonable to conclude that the FJH process is highly

scalable, with the capability for industry-scale application.

FJH工艺在我们实验室的规模化演示。
The demonstration of the scaling of the FJH process in our research lab.

在我们的典型实验中，我们使用的质量为m0=0.2 g，FJH条件为V0=150 V，C0=0.06 F。在此，我们
In our typical experiment, we use a mass of m_0 = 0.2 g, with the FJH condition of V_0 = 150
展示了FJH按比例放大到每批质量为m1=2 g，m2=4 g的比例(补充图23a)。
V and C_0 = 0.06 F. Here, we demonstrate the scaling up of FJH to a scale with mass of m_1 = 2
我们使用了由104个铝电容器(6 mF，450
g and m_2 = 4 g per batch (**Supplementary Fig. 23a**). We used a capacitor bank composed of
V，Mouser#80-PEH200YX460BQU2)并联组成的电容器组，因此总电容为C1=0.624 F。
104 aluminum capacitors (6 mF, 450 V, Mouser #80-PEH200YX460BQU2) in parallel, so the
对于m1=2 g的样品质量，我们使用V1=150 V的FJH电压，对于m1=2
total capacitance is C_1 = 0.624 F. For the sample mass of m_1 = 2 g, we use a FJH voltage of V_1
g的样品质量，我们使用V2=300 V的FJH电压，因此这些条件符合等式S19的标度规则。由于温度是蒸发分离
= 150 V, and for the sample mass of m_1 = 2 g, we use a FJH voltage of V_2 = 300 V, thus these
方案中ewaste处理的关键参数，我们记录了这些样品的温度(补充图)。
conditions fit with the scaling rule of **eq S19**. Since temperature is a key parameter for the e-

waste processing in our evaporative separation scheme, we recorded the temperature for those
发现所有样品的温度都达到3000 K以上，表明FJH工艺的有效
samples (**Supplementary Figs. 23b-d**). It is found that the temperature reaches >3000 K for
放大。
all the samples, demonstrating the effective scaling up of the FJH process.

对FJH工艺连续处理电子废物的循证预测。

The evidence-based prediction of the continuous processing of e-waste by the FJH process.

除了逐批处理外，我们还对FJH处理电子废物的连续处理模式进行了循证预测。

In addition to the batch-by-batch process, we made evidence-based predictions for the continuous processing mode of the FJH processing of e-waste. As shown in **Supplementary Fig. 24**, two baffles separate the feeds and the remaining solid. After the FJH, the bottom baffle is opened and the remaining solid is removed from the reactor. The top baffle is then opened, and the feeds are loaded into the reactor for the next FJH reaction. Since the collected volatiles in the cold trap are very little per FJH, it is not necessary to change the collection vessel. Note that this is only one possible continuous production method. Many mature engineering practices could be applied.

如补充图24所示，两个挡板将进料和剩余固体隔开。FJH后，底部挡板打开，剩余固体从反应器中移除。然后打开顶部挡板，将进料装入反应器中，进行下一个FJH反应。由于每个FJH冷阱中收集的挥发物很少，因此无需更换收集容器。请注意，这只是一种可能的连续生产方法。可以应用许多成熟的工程实践。

FJH工艺的工业规模应用正在进行中。

Industrial-scale application of the FJH process is underway.

FJH工艺是我们集团发明的用于合成闪光石墨烯9的工艺，目前已由环球物质公司(Universal Matter, Inc.)进行工业规模的扩大(https://www.universalmatter.com/).

The FJH process, which was invented by our group for the synthesis of flash graphene[9], is already undergoing industrial-scale scaling up by Universal Matter, Inc (https://www.universalmatter.com/). The equipment and process developed and optimized for the flash graphene synthesis are ready to be shifted for the processing of e-waste. The evaporative separation system consisted of the FJH and the gas collection setups. The gas collection setup uses a cold trap with a mild vacuum, which should be scalable by using a larger vessel and mechanical pump.

为快速石墨烯合成开发和优化的设备和工艺已准备好转移到电子废物处理中。蒸发分离系统由FJH和气体收集装置组成。气体收集装置使用具有轻度真空的冷阱，应通过使用更大的容器和机械泵进行扩展。

补充数字

Supplementary Figures

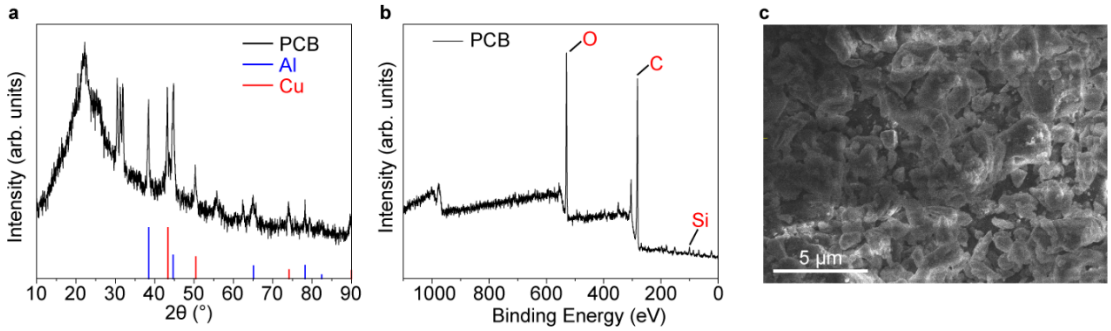

补充图1 |印刷电路板(PCB)粉末的特性。

Supplementary Fig. 1 | Characterization of the printed circuit board (PCB) powder. (a) PCB粉末的X射线衍射(XRD)。铝和铜是PCB原材料中的丰富金属。X-ray diffraction (XRD) of the PCB powder. Al and Cu are abundant metals in PCB raw materials. (b) (b) PCB粉末的X射线光电子能谱(XPS)全谱。X-ray photoemission spectroscopy (XPS) full spectrum of PCB powder. (c) (c) 机械锤磨后PCB粉末的扫描电子显微镜(SEM)。Scanning electron microscopy (SEM) of the PCB powder after mechanical hammer grinding.

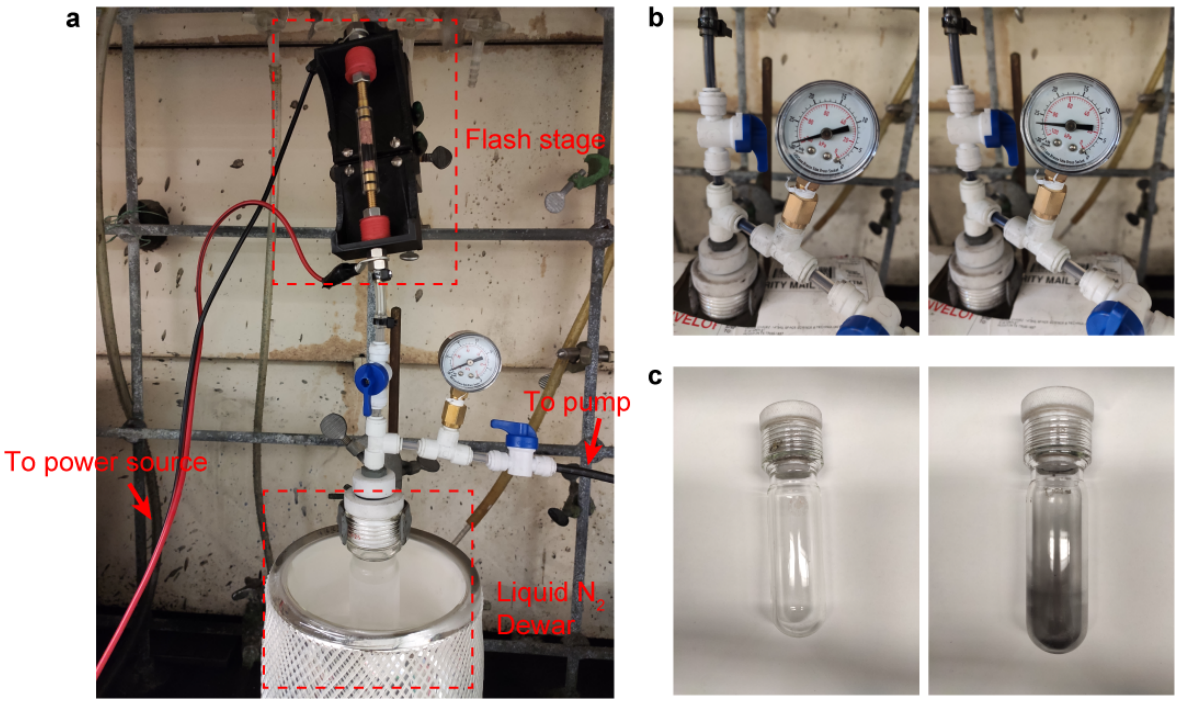

补充图2 |收集蒸发金属蒸汽的系统图片。

Supplementary Fig. 2 | Picture of the system to collect the evaporated metal vapor. (a) 蒸发收集系统的图片。 (b) 闪光焦耳加热(FJH)前后的真空计图片。 Picture of the evaporative collection system. (b) Picture of the vacuum gauge before and after flash Joule heating (FJH). (c) 闪光焦耳加热(FJH)反应前后冷凝容器的图片。 (c) Picture of the condensate vessel before and after the FJH reaction.

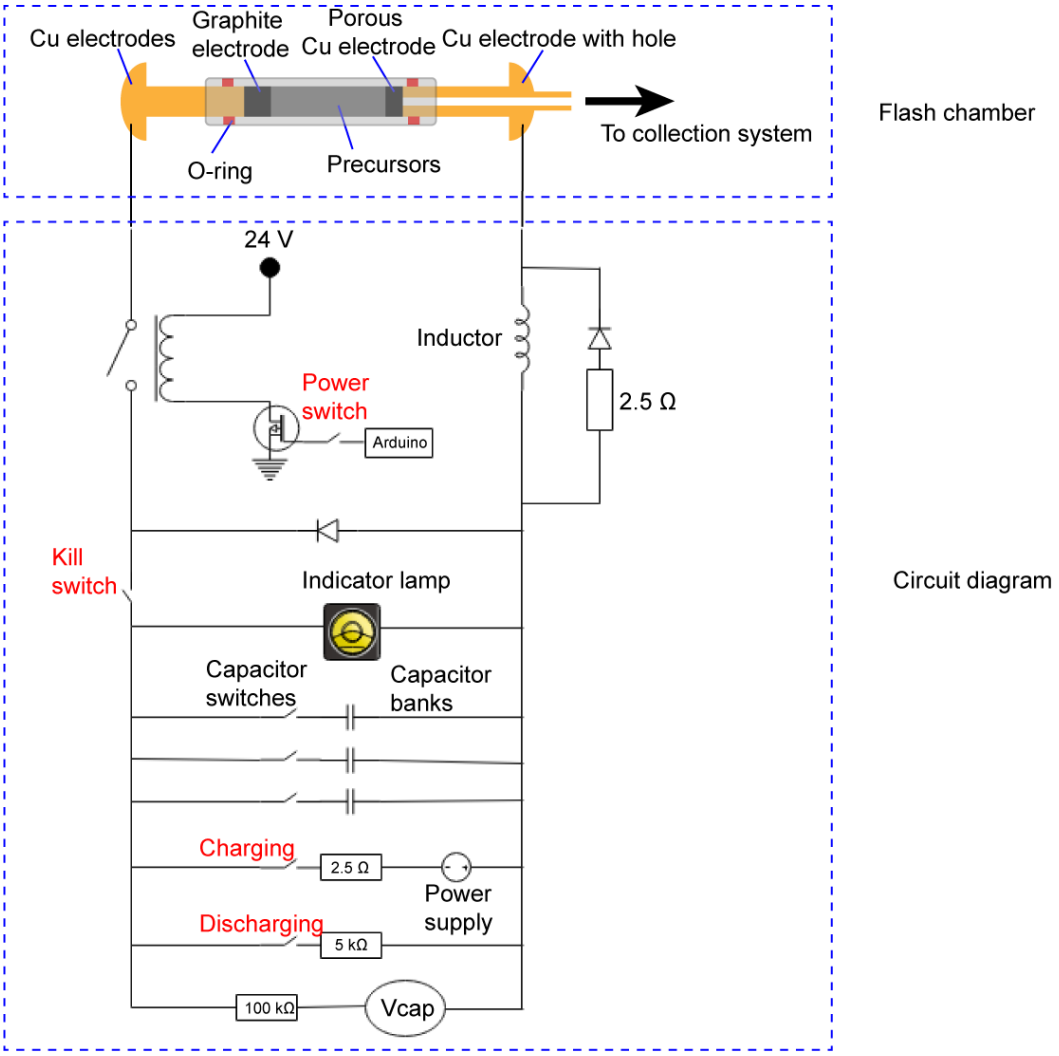

补充图3 |闪光焦耳加热(FJH)系统的电路图。

Supplementary Fig. 3 | Electrical circuit diagram of the flash Joule heating (FJH) system.

电容器组的总电容为60 mF。有关电气组件的更多详细信息，请参阅我们之前的出版物9。

The total capacitance of the capacitor bank is 60 mF. More details about the electrical components could be found in our previous publications[9].

警告：如果操作不当，有触电的风险。建议使用焊接用安全玻璃，以阻挡闪光反应期间的红外光和紫外线。

CAUTION: There is a risk of electrical shock if improperly operated. Safety glasses for welding are recommended to block the infrared and ultraviolet light during the flashing reaction. 系统内置了许多安全措施。但是，作为最后一个注意事项，应遵守单手规则(不要用双手触碰仪器，防止出现任何问题时通过身体的电路闭合)和厚橡胶

There are numerous safety measures built into the system. But, as a final level of caution, the “one hand rule” should be obeyed (do not touch the apparatus with both hands, preventing the closing of a circuit through your body if anything goes wrong), and thick rubber

应使用延伸至肘部的手套。 更多安全实施可以在我们之前的出版物9-11中找到，
gloves that extend to the elbows should be used. More safety implementations can be found in
我们也在下面列出了这些出版物。
our previous publications[9-11], which we also listed below.

FJH工艺安全指南。
Safety guidance of the FJH process.

1、封闭或小心绝缘所有接线。
1. Enclose or carefully insulate all wire connections.

所有连接、导线和部件必须适合高电压和高电流。
2. All connections, wires, and components must be suitable for the high voltages and currents.

单手定则。 在系统上工作时，只需一只手，另一只手不要接触任何接地表面。
3. One hand rule. Use only one hand when working on the system, with the other hand not touching any grounded surface.

提供一个机械放电断路器开关，该开关连接到几百欧姆的功率电阻器，以快速释放电容器电荷。
4. Provide a mechanical discharge circuit breaker switch connected to a power resistor of a few hundred ohms to rapidly bleed off the capacitor charge.

提供压井断路器开关，以断开样品架与电容器组的连接。
5. Provide a “kill” circuit breaker switches to disconnect the sample holder from the capacitor bank.

6.在设备上张贴高压警告标志。
6. Post high voltage warning signs on the apparatus.

7、请记住，系统可以在毫秒内放电数千焦耳，这可能导致继电器等部件发生故障。
7. Keep in mind that the system can discharge many thousands of Joules in milliseconds, which can cause components such as relays to explore.

始终将带有高压测试引线的电压表放在手边。 在电容器组上工作时，务
8. Keep a voltmeter with high voltage test leads handy at all times. When working on the
必检查每个电容器组上的电压。
capacitor bank, always check the voltage on each.

9、使用仪器时，戴上厚厚的橡胶手套，以防触电。
9. Wear thick rubber gloves when using the apparatus to protect from electrocution.

所有用户均应由经验丰富的电气技术人员进行适当培训。
10. All users should be properly trained by an experienced electrical technician.

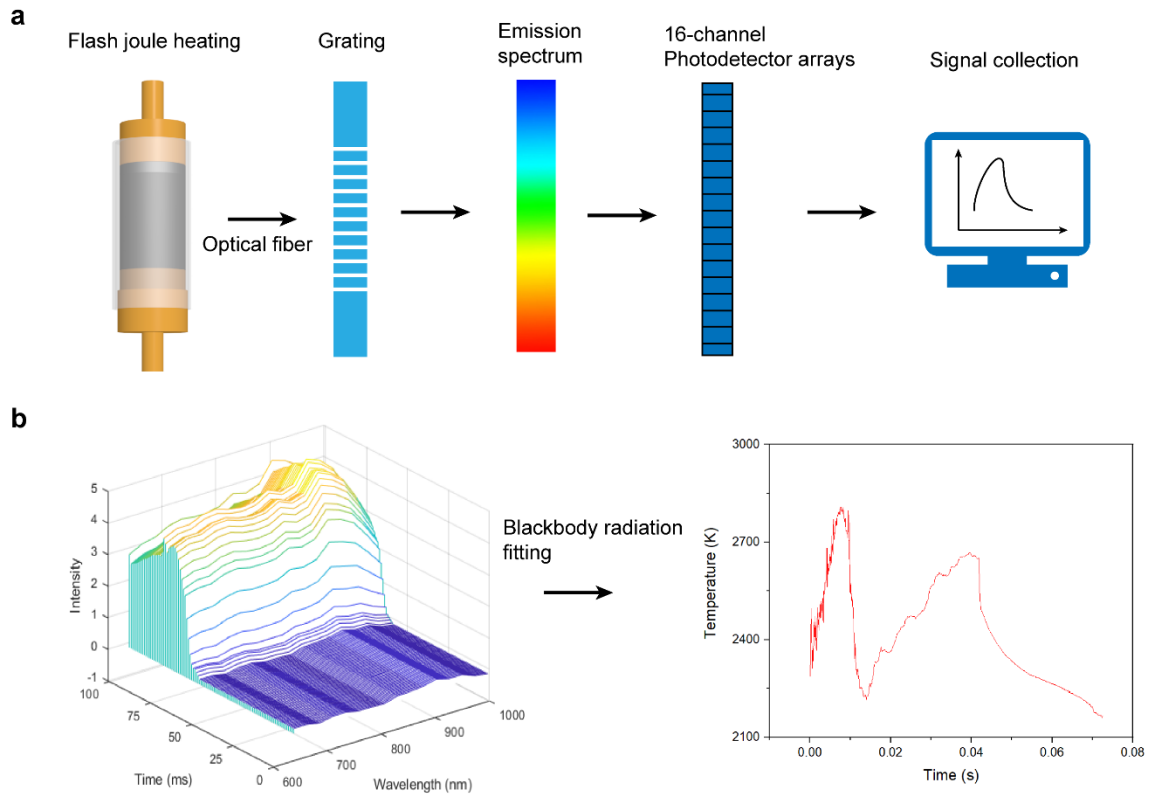

补充图4 |通过拟合黑体进行时间分辨温度测量

Supplementary Fig. 4 | Time-resolved temperature measurement by fitting the blackbody radiation. (a) Schematic configuration of the time-resolved pyrometer for spectrum collection during the flash Joule heating (FJH) process. Black body radiation from the sample during FJH is collected by an optical fiber and separated by a customized grating black box. The spectrum radiance was recorded using a 16 pixels photodiode array (Hamamatsu S4111-16R) at 600 – 1100 nm. The reversed bias voltages from the photodiode arrays are collected by a National Instrument multifunction I/O device PCIe-6320. (b) Temperature determination by fitting of the black body radiation. The spectra were fitted to the blackbody radiation equation to acquire a time-resolved temperature of the sample. Prior to measurement, the temperature was calibrated by using a 2800 K lamp.

（a）闪光焦耳加热（FJH）过程中用于光谱采集的时间分辨高温计的示意图配置。FJH期间样品的黑体辐射通过光纤收集，并通过定制的光栅黑箱进行分离。使用16像素光电二极管阵列（Hamamatsu S4111-16R）在600 1100 nm处记录光谱辐射。来自光电二极管阵列的反向偏置电压由国家仪器多功能输入/输出设备PCIe-6320收集。（b）通过黑体辐射拟合确定温度。将光谱拟合到黑体辐射方程，以获得样品的时间分辨温度。测量之前，使用2800 K灯校准温度。

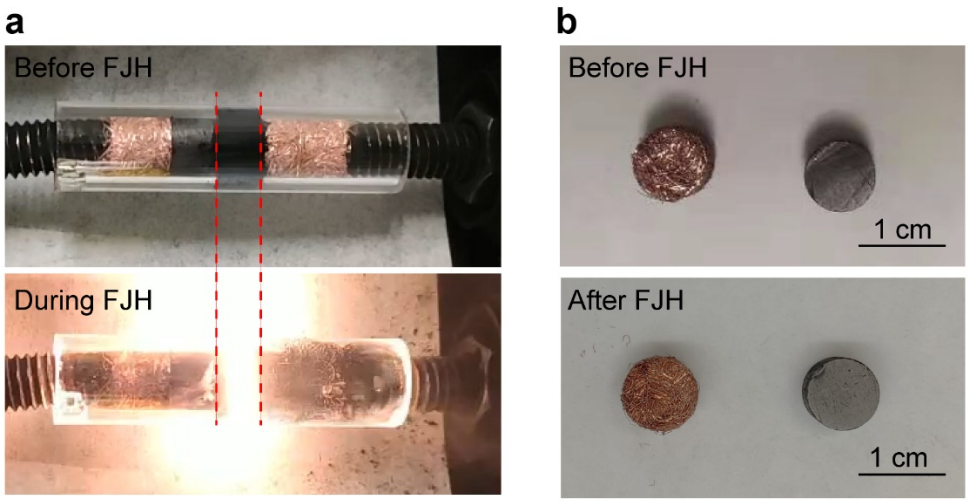

补充图5。闪光焦耳加热(FJH)设置的耐久性。(a)的图像

Supplementary Fig. 5. Durability of the flash Joule heating (FJH) setup. (a) Image of the

FJH之前和期间的样品。(b) FJH前后多孔铜电极(两张照片中的左侧)和石墨电极(

sample before and during FJH. (b) Images of the porous Cu electrode (on the left in both

两张照片中的右侧)的图像。

photos) and graphite electrode (on the right in both photos) before and after FJH.

FJH工艺可以达到高温，但高温区域仅限于样品。

The FJH process could achieve a high temperature, but the high-temperature region is

根据焦耳加热公式，=：，热量与电阻成正比。

limited to the sample. According to the Joule heating formula, $Q = I^2Rt$, the heat amount is

铜电极、石墨电极和样品的电阻值分别约为0.09、0.11和>2.0。

proportional to the resistance. The resistance values of the Cu electrode, the graphite electrode,

铜电极和石墨电极的电导率比样品高

and the sample are ~0.09 Ω, ~0.11 Ω, and >2.0 Ω, respectively. The Cu and graphite electrodes

得多。因此，电压降主要施加在样品上，放电产生的热量主

have much higher conductivity than the sample. Hence, the voltage drop was mainly imposed

要保留在样品上。

on the sample, and the heat amount generated by the discharging mostly retains on the sample.

在FJH期间，强发光区域仅限于样品(补充图5a)，表明铜和石墨电极保持低温。

During the FJH, the strong light emission region is limited to the sample (**Supplementary Fig.**

铜电极的高导热性也

5a), indicating that Cu and graphite electrodes remain low temperature. The high thermal

有助于快速散热并防止高温。

conductivity of the Cu electrodes also helps the fast thermal dissipation and prevents the high

此外，FJH时间很短，在几十毫秒内温度>3000 K。

temperature. Moreover, the FJH time is very short, with the >3000 K temperature in tens of

FJH后，除了铜电极被CB污染外，铜电极和石墨棒没有明显变化(补充图5b)。

ms. The Cu electrode and graphite rod show no obvious change after the FJH other than the

铜的电阻

contamination of the Cu electrode by CB (**Supplementary Fig. 5b**). The resistance of the Cu

FJH后，电极和石墨电极保持不变。因此，FJH工艺对铜和石墨
electrodes and the graphite electrodes remains the same after the FJH. Hence, the FJH process
电极没有显著影响。
has no significant effect on the Cu and graphite electrodes.

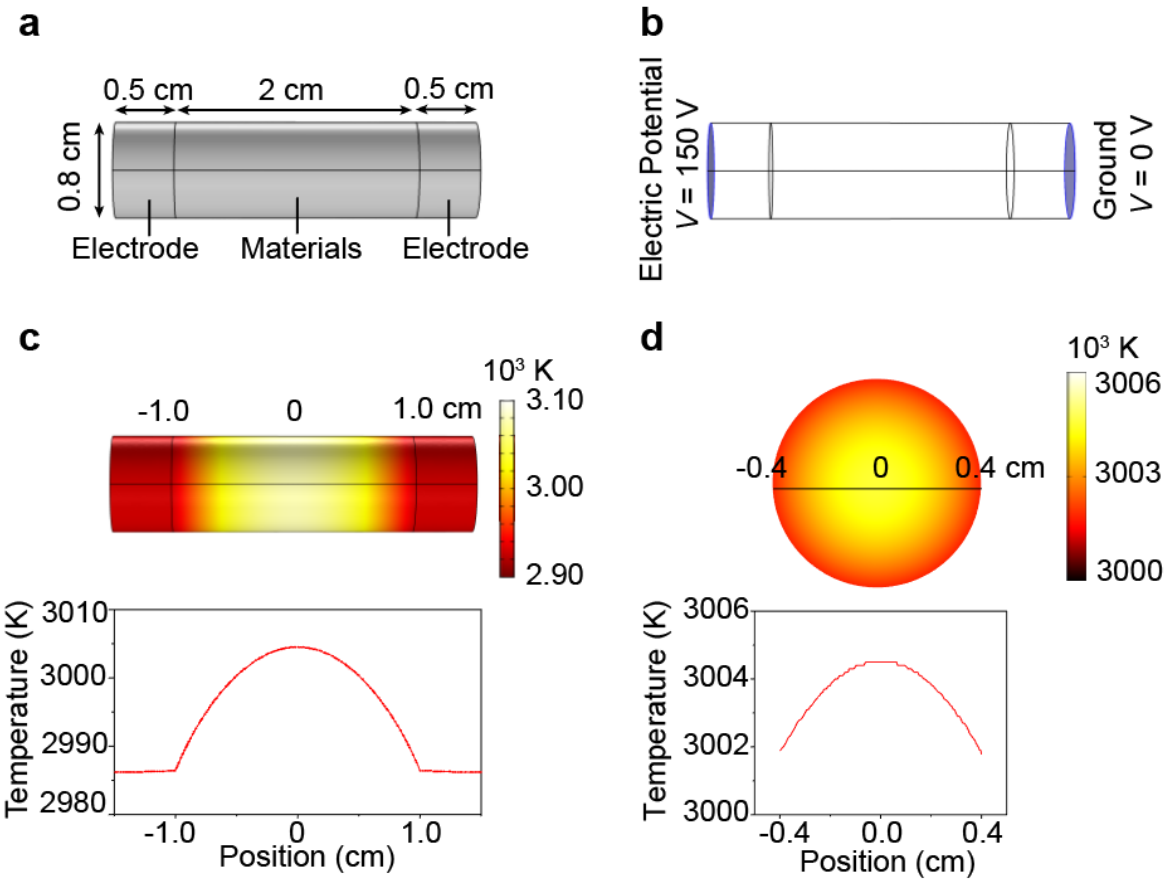

补充图6 |温度模拟。(a) 几何参数。(b) 边界
Supplementary Fig. 6 | Temperature simulation. (a) Geometrical parameters. (b) Boundary
条件 (c) 样品沿纵向的温度分布和温度分布。
conditions. (c) Temperature distribution and the temperature profile of the sample along the
(d) 样品沿径向的温度分布和温度分布。
longitudinal direction. (d) Temperature distribution and the temperature profile of the sample
结果表明，闪光焦耳加热(FJH)在纵向和径向都是均匀的。
along the radial direction. The results show that the flash Joule heating (FJH) is homogenous
both in the longitudinal and the radial directions.

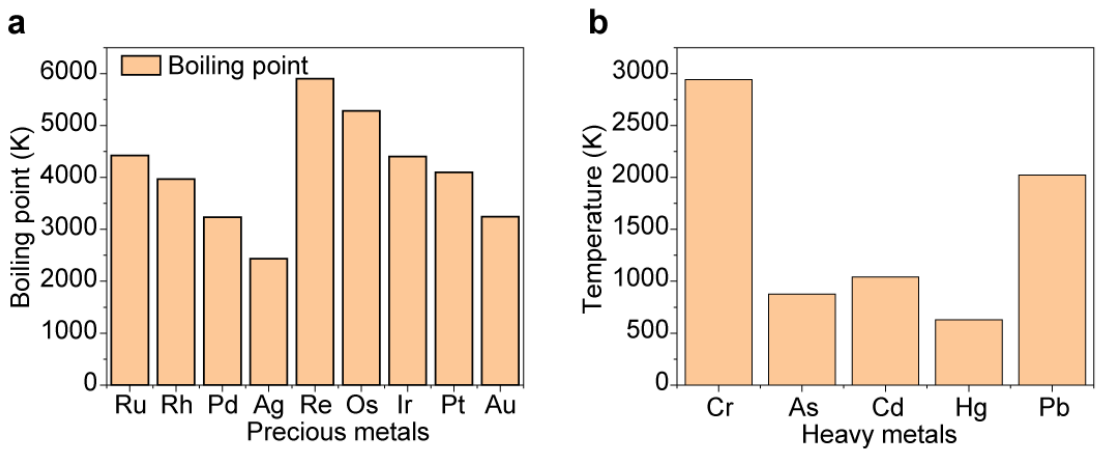

补充图7 |贵金属和重金属的沸点。

Supplementary Fig. 7 | The boiling points of (a) precious metals and (b) heavy metals.

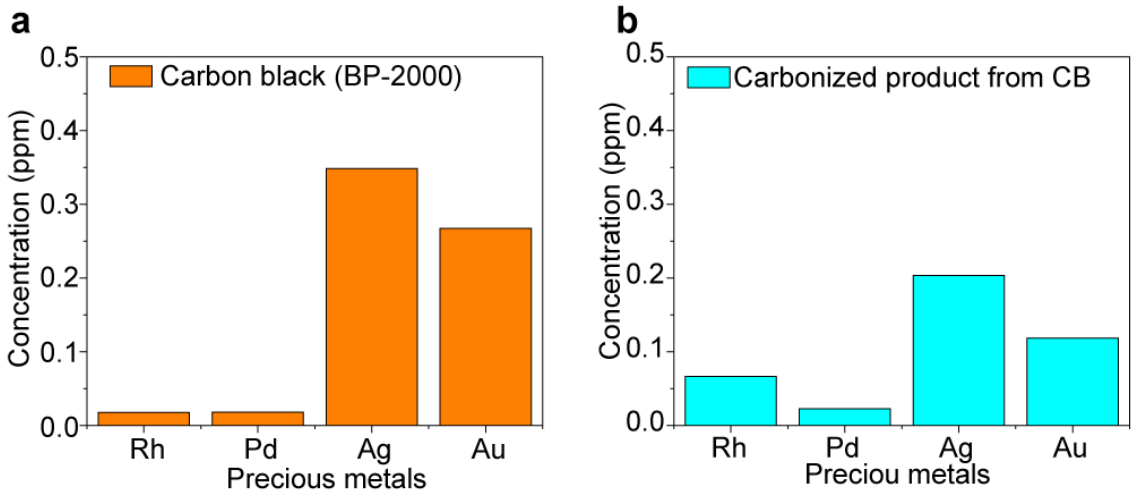

补充图8 |炭黑(CB)中的贵金属浓度。(a) 珍贵的

Supplementary Fig. 8 | Precious metals concentration in carbon black (CB). (a) Precious

CB中的金属浓度(BP-2000)。(b) CB(BP-2000)闪速焦耳加热(FJH)碳化产物

metals concentration in CB (BP-2000). (b) Precious metals concentration in the carbonized

中的贵金属浓度。CB中的贵金属浓度约为印

product obtained from flash Joule heating (FJH) of CB (BP-2000). The concentration of

刷电路板(PCB)中贵金属浓度的12%。

precious metals in CB are ~1 – 2% of those in printed circuit board (PCB).

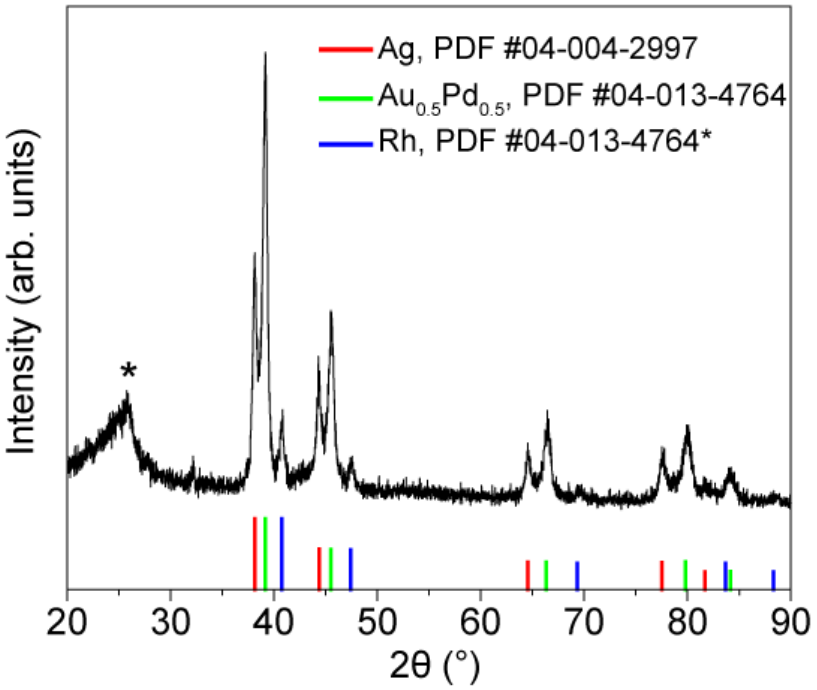

补充图9。闪速焦耳加热(FJH)后RhCl3、PdCl2、AgCl、HAuCl4和炭黑(CB)混合物的X射线衍射(XRD)图谱。峰值(*)表示石墨(0002)由于炭黑的石墨化。

Supplementary Fig. 9. X-ray diffraction (XRD) pattern of the mixture of $RhCl_3$, $PdCl_2$, AgCl, $HAuCl_4$ and carbon black (CB) after flash Joule heating (FJH). The peak (*) denotes the graphite (0002) due to the graphitization of the CB.

贵金属作为后过渡族金属，通常与C的亲和力较弱，对碳几乎没有溶解性。贵金属即使在高温下也不会形成碳化物相12。例如，没有实验证据表明可能存在无机结晶金碳化合物。在实验上，我们将RhCl3、PdCl2、AgCl和HAuCl4与CB(各5 wt%)混合，并进行FJH。产品的XRD图谱如补充图9所示。XRD结果表明，样品中存在纯金属相和金属合金相。未观察到贵金属碳化物相。因此，使用CB作为导电添加剂不会影响贵金属的蒸发行为。

The precious metals as the late transition group metals usually have weak affinity with C and almost no solubility for carbon. The precious metals tend to not form carbide phases even at high temperature[12]. For example, there is no experimental evidence for a possible inorganic crystalline gold carbon compound. Experimentally, we mixed $RhCl_3$, $PdCl_2$, AgCl, and $HAuCl_4$ with CB (5 wt% for each) and conducted the FJH. The XRD pattern of the product is shown in **Supplementary Fig. 9**. The XRD result showed that there were pure metal phases and metal alloy phases. No precious metal carbide phase was observed. Hence, the use of CB as conductive additives will not affect the evaporative behavior of precious metals.

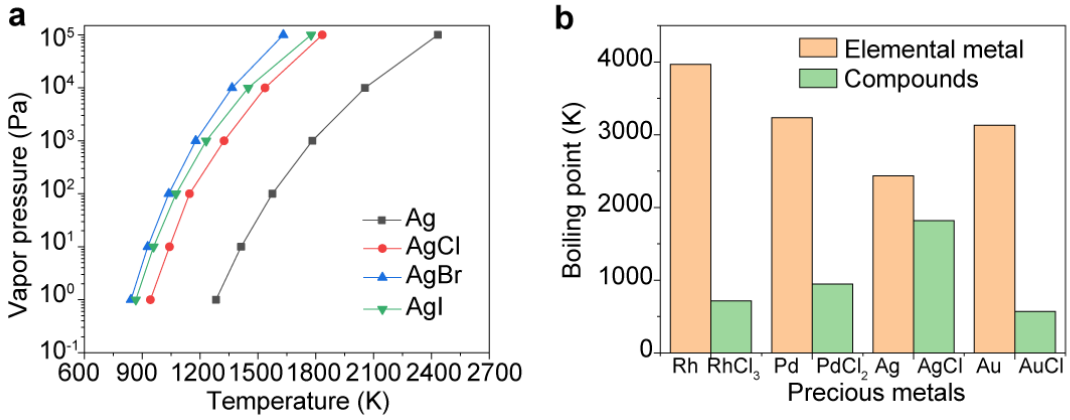

补充图10 |金属卤化物的蒸气压和沸点。（a）蒸汽

Supplementary Fig. 10 | Vapor pressure and boiling point of metal halides. (a) Vapor

银和卤化银的压力-温度关系13。（b）元素金属和金属氯化物的沸点13。注意，PdCl2沸点是分解温度

pressure-temperature relationships of Ag and Ag halides[13]. (b) Boiling points of elemental

。

metals and metal chlorides[13]. Note that the $PdCl_2$ boiling point is the decomposition

temperature.

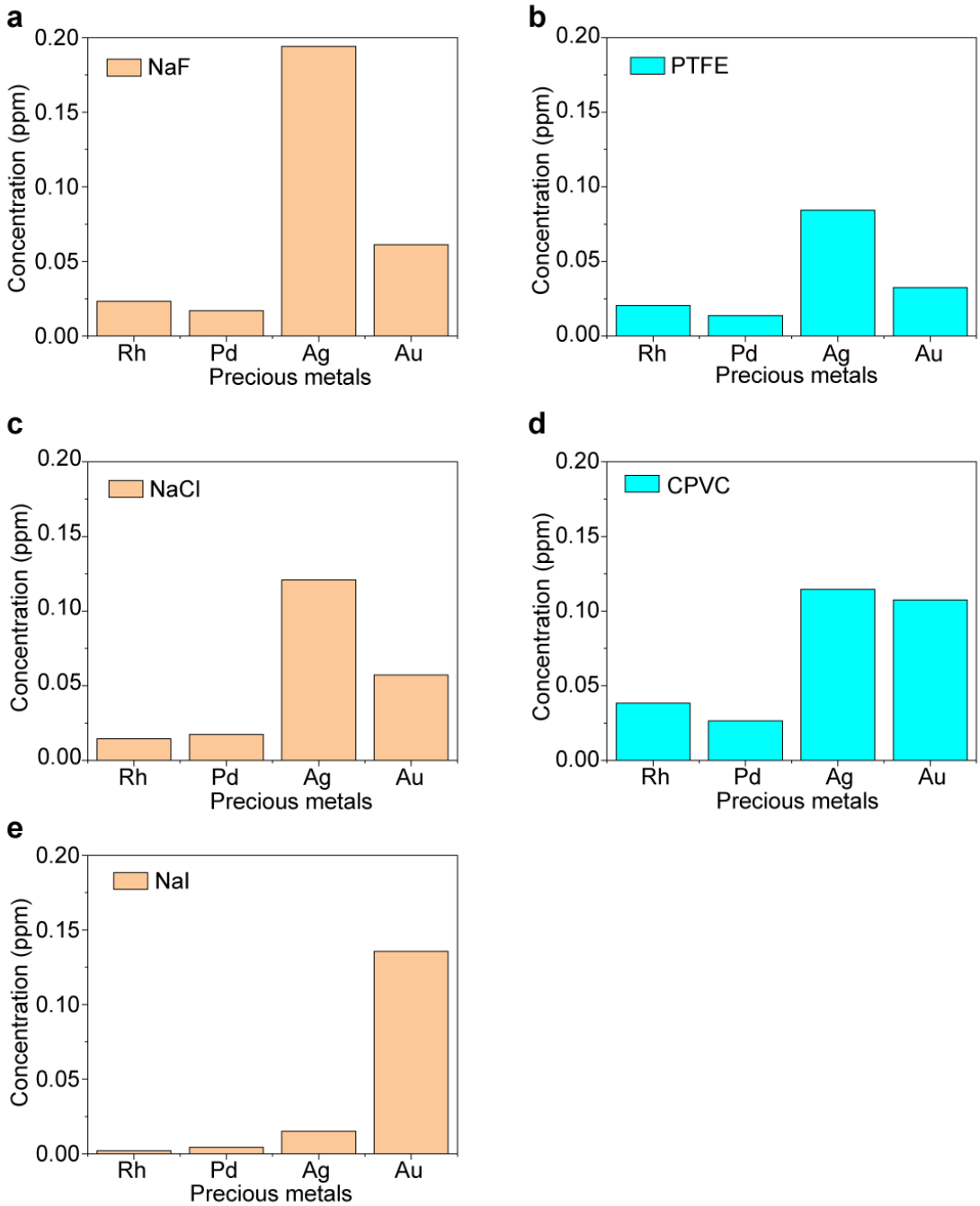

补充图11 |添加剂中贵金属的浓度。

Supplementary Fig. 11 | Concentration of precious metals in additives. (a) NaF. (b) PTFE. (c) NaCl. (d) CPVC. (e) NaI. The concentration of precious metals in those additives are <1% of those in printed circuit board (PCB) raw materials.

这些添加剂中的贵金属浓度小于印刷电路板(PCB)原材料中贵金属浓度的1%。

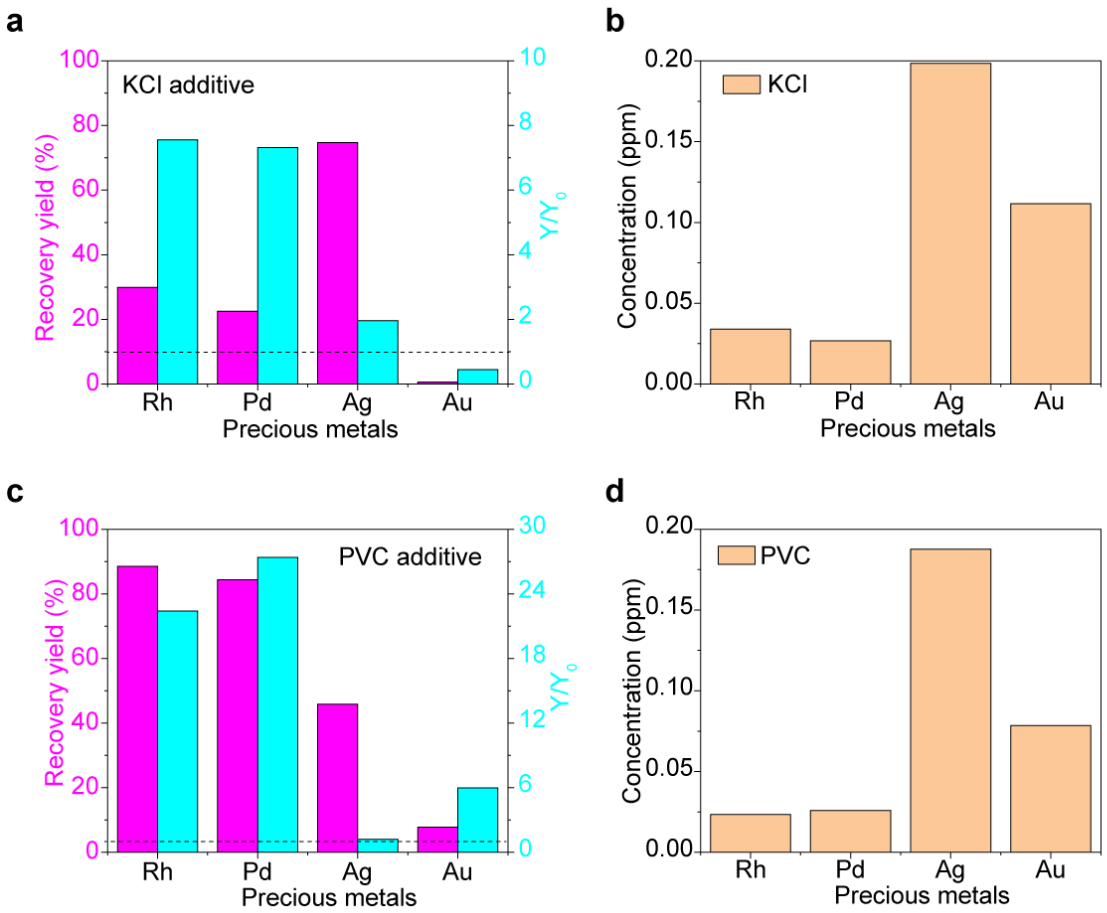

补充图12 |使用氯化物添加剂提高回收率。

Supplementary Fig. 12 | Recovery yield improvement by using chloride additives. (a) 使用KCl添加剂提高回收率。 (b) KCl中贵金属的浓度。 (c) 使用聚氯乙烯(PVC)添加剂提高回收率。 (d) PVC中贵金属的浓度。 应小心使用这些金属盐，因为对金属进行碳热还原可获得可在水或潮湿空气中燃烧的金属(0)，尽管我们从未观察到这种规模的问题。

Increase in recovery yield using KCl additive. (b) Concentration of precious metals in KCl. (c) Increase in recovery yield by using polyvinyl chloride (PVC) additive. (d) Concentration of precious metals in PVC. Care should be taken with these metal salts since carbothermal reduction to the metal can occur to afford metal(0) that can combust in water or moist air, though we never observed that problem at this scale.

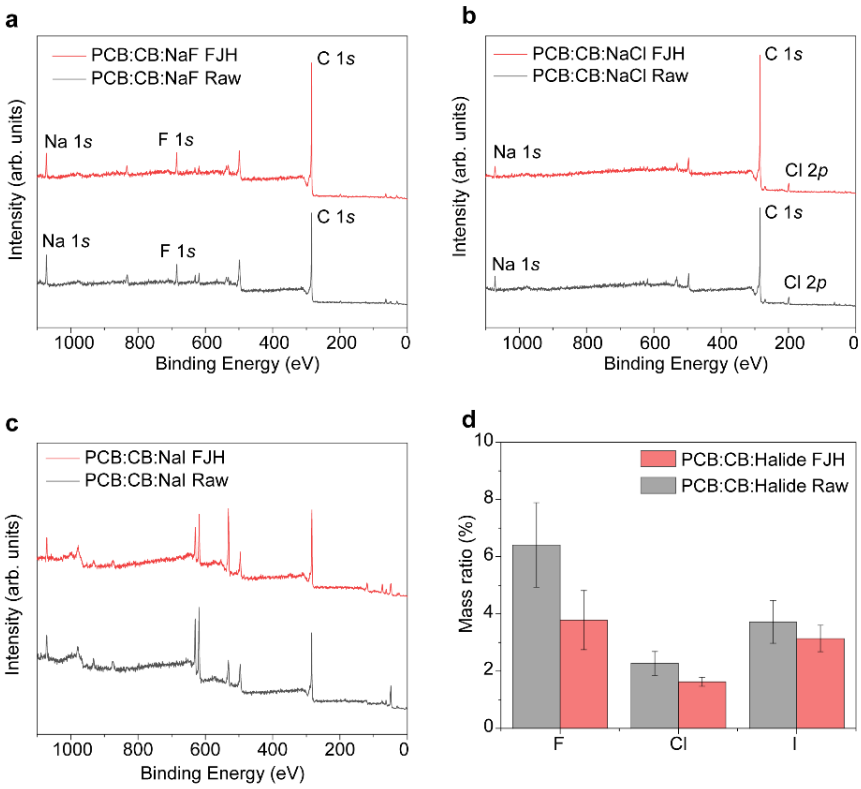

补充图13。 闪光焦耳加热过程中卤化物的蒸发损失

Supplementary Fig. 13. The evaporative loss of halides during the flash Joule heating

(FJH)过程。 (a)X射线光电子能谱(XPS)显示了氟化钠添加剂在FJH前后样品的全光谱。

(FJH) process. (a) X-ray photoemission spectroscopy (XPS) full spectra of the sample with

(b)FJH前后加入NaCl添加剂样品的XPS全谱图。

NaF additives before and after FJH. (b) XPS full spectra of the sample with NaCl additives

(c)FJH前后加入NaI添加剂样品的XPS全谱图。

before and after FJH. (c) XPS full spectra of the sample with NaI additives before and after

(d)FJH前后卤化物添加剂的质量比。

FJH. (d) The mass ratios of halide additives before and after FJH.

原料中卤化物的质量比为F，约6.4%；氯，约2.3%；而我，大约3.7%。 FJH后

The mass ratios of halide in the raw materials were F, ~6.4%; Cl, ~2.3%; and I, ~3.7%. After

，剩余固体中的卤化物含量为F，约为3.8%；氯，约1.6%；而我，大约3.1%。 这相

FJH, the halide content in the remaining solids was F, ~3.8%; Cl, ~1.6%; and I, ~3.1%. This

当于F的蒸发损失，约为40%；氯，约30%；而我，大约16%。 卤化物盐由于其高溶解

corresponds to the evaporative loss of F, ~40%; Cl, ~30%; and I, ~16%. The halide salts are

度，预计可通过水洗和沉淀过程轻松回收，而电子废物和碳的成分水溶性较低(如有)。

expected to be easily recovered by a water washing and precipitation process due to their high

solubility, while the components of the e-waste and carbon have low water solubility if any.

因此，可以回收固体中残留的卤化物，或在冷阱中蒸发和收集的卤化物。

Hence, it is possible to recovery the halides either remaining in the solids or evaporated and

卤化物的使用不会带来显著的额外材料成本。

collected in the cold trap. The use of the halides will not introduce significant additional

materials cost.

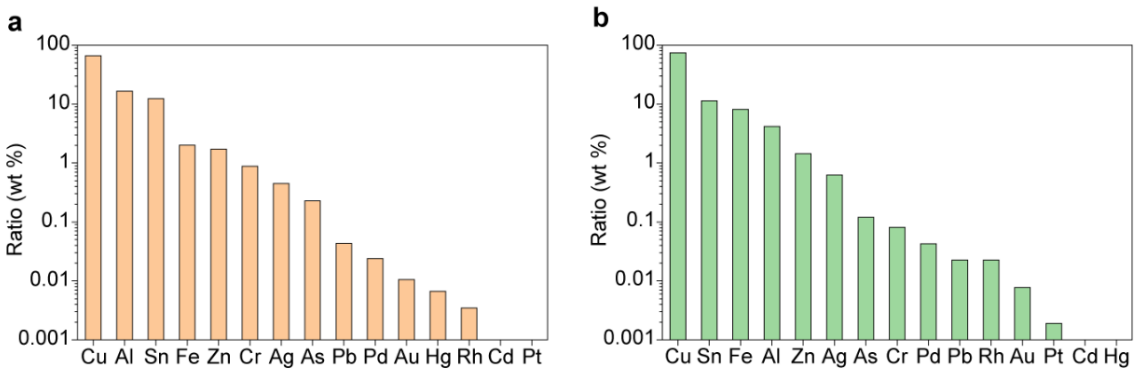

补充图14。收集固体的总成分分析。（a）金属质量不含添加剂的收集固体中15种元素的比率。（b）混合添加剂NaF、NaCl和NaI收集的固体中15种元素的金属质量比。

Supplementary Fig. 14. Total composition analysis of the collected solid. (a) Metal mass ratios of 15 elements in the collected solid without additive. (b) Metal mass ratios of 15 elements in the collected solid with the mixture additives NaF, NaCl, and NaI.

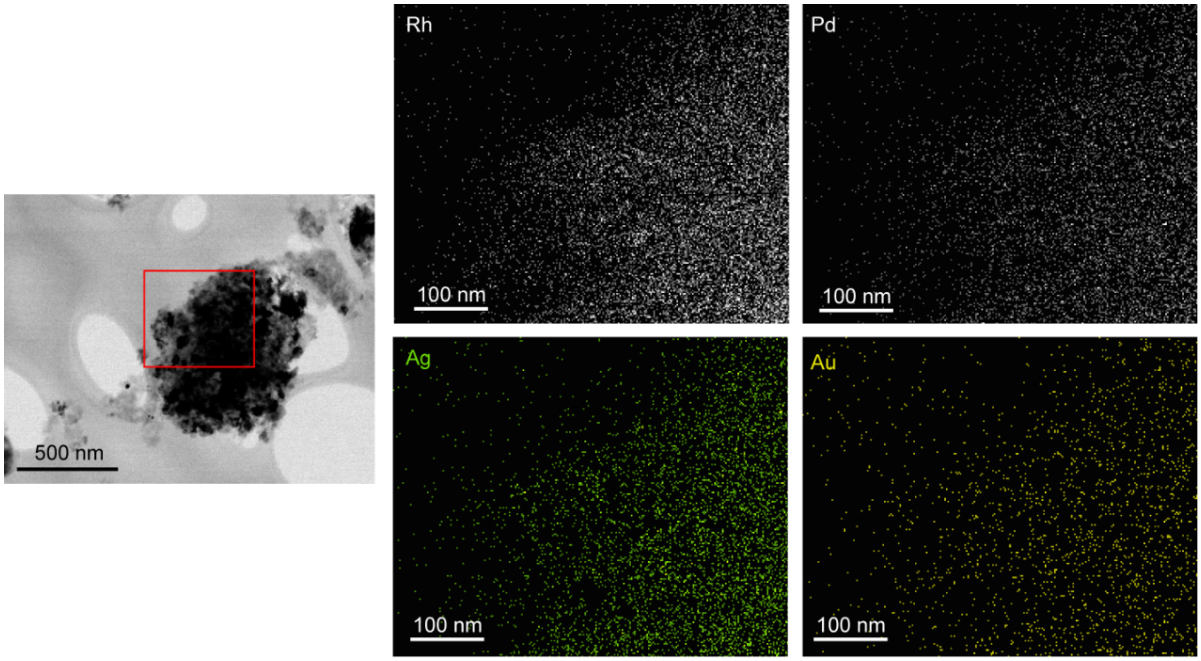

补充图15 |收集的固体的扫描透射电子显微镜(STEM)图像和Rh、Pd、Ag和Au的能量色散光谱(EDS)图。

Supplementary Fig. 15 | Scanning transmission electron microscopy (STEM) image of the collected solid and Energy dispersion spectroscopy (EDS) maps of Rh, Pd, Ag, and Au.

元素图证明了贵金属的成功采集。金属分布在整个收集的固体上。

The element maps prove that the successful collection of precious metals. The metals spread over the entire collected solid.

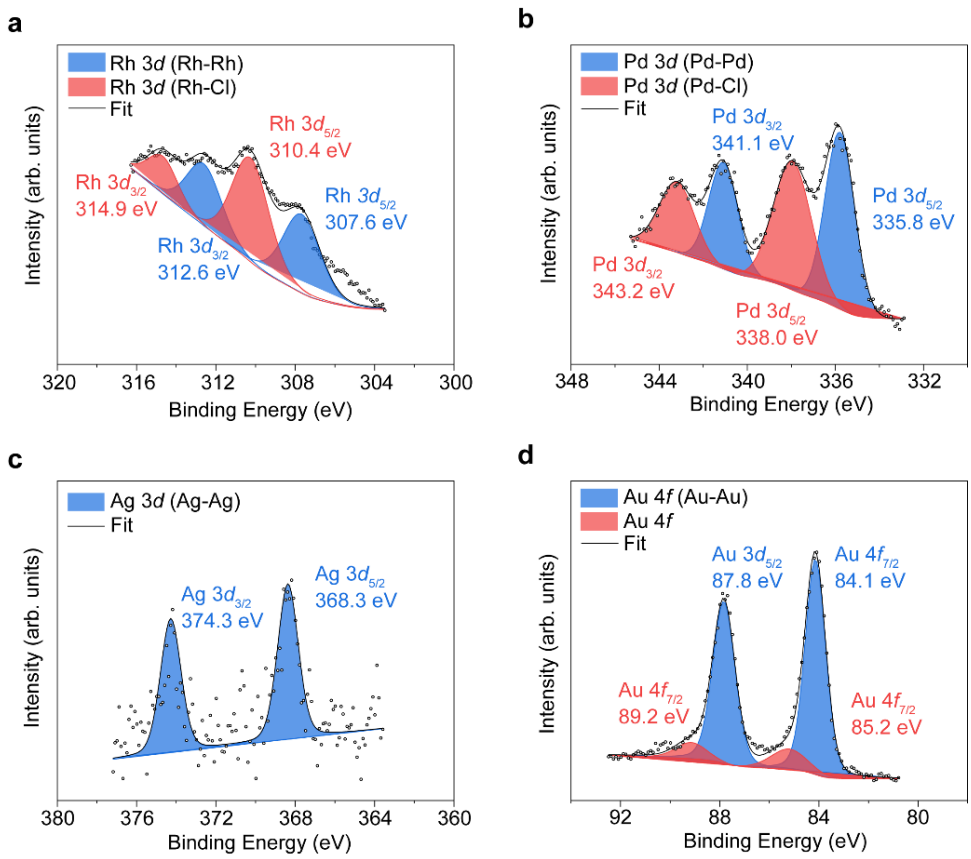

补充图16。收集固体的化学状态分析。(a) X射线

Supplementary Fig. 16. Chemical state analysis of the collected solids. (a) X-ray

Rh的光电子能谱(XPS)精细光谱。(b) 钯的XPS精细光谱。(c)

photoemission spectroscopy (XPS) fine spectrum of Rh. (b) XPS fine spectrum of Pd. (c) XPS

银的XPS精细光谱。(c) 金的XPS精细光谱。

fine spectrum of Ag. (c) XPS fine spectrum of Au.

由于贵金属含量<0.1 wt%(补充图14)，很难通过XPS直接分析。

Since the contents of precious metals are <0.1 wt% (**Supplementary Fig. 14**), it is difficult to

在这里，我们将RhCl3、PdCl2、AgCl和HAuCl4添加到电子废物和CB的混合物中(

directly analyze by XPS. Here, we added $RhCl_3$, $PdCl_2$, AgCl, and $HAuCl_4$ into the mixture of

每种重量百分比为5%)，并执行相同的FJH过程，收集挥发物进行XPS分析。

e-waste and CB (5 wt% for each) and conducted the same FJH process and collected the

贵金属的XPS精细光谱如补充图16所示。

volatiles for XPS analyses. The XPS fine spectra for precious metals were shown in

Ag和Au主要以元素状态存在。Au 4f7/2在85.2

Supplementary Fig. 16. The Ag and Au were mainly in the elemental state. The minor peak

eV处的副峰可能来自Au基金属合金，例如AuIn214。Rh和Pd均

at 85.2 eV for Au $4f_{7/2}$ could be from the Au-based metal alloy, for example, $AuIn_2$[14]. For Rh

存在元素态和氧化态。310.4 eV处的Rh 3d5/2峰值可分配给RhCl315

and Pd, both elemental and oxidation states existed. The Rh $3d_{5/2}$ peak at 310.4 eV could be

，338.0 eV处的Pd 3d5/2峰值可分配给PdCl216。这种差

assigned to $RhCl_3$[15], and the Pd $3d_{5/2}$ peak at 338.0 eV could be assigned to $PdCl_2$[16]. This

异可能归因于贵金属的不同化学反应性。

difference might be attributed to the different chemical reactivity of the precious metals.

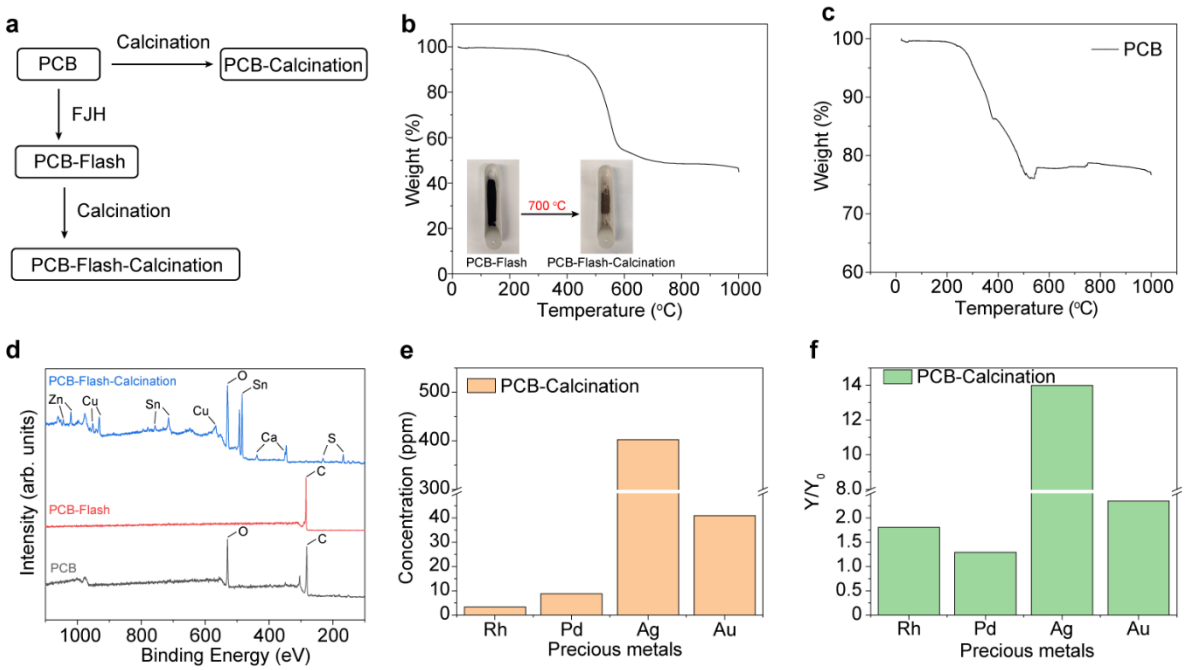

补充图17 |通过闪光焦耳加热(FJH)和煅烧。(a)从印刷电路板(PCB)中回收贵金属的不同工艺。

Supplementary Fig. 17 | Recovery of precious metal by flash Joule heating (FJH) and calcination. (a) Different processes for the recovery of precious metals from printed circuit board (PCB). (b) Thermogravimetric analysis (TGA) curve of PCB-Flash in air. Inset, the picture of PCB-Flash, and PCB-Flash-Calcination. The TGA curve shows that the PCB-Flash started to lose weight at ~400 °C and remains stable at ~800 °C. (c) TGA curve of PCB. (d) X-ray photoemission spectroscopy (XPS) of PCB, PCB-Flash, and PCB-Flash-Calcination. The XPS of PCB shows mostly C and some inorganic signals. The XPS of PCB-Flash shows mostly C signals, indicating that O was removed by the FJH process, and the inorganic element peaks are not detected, presumably because the inorganics were covered by carbon during the FJH process. The XPS of PCB-Flash-Calcination show abundant elemental signals, demonstrating the removal and exposure of inorganic materials. (e) Concentration of precious metals in PCB-Calcination. (f) Improvement of leaching yield by calcination. Y_0 and Y mean the recovery yield by leaching PCB and PCB-Calcination, respectively.

(b)PCB在空气中闪蒸的热重分析(TGA)曲线。插图、PCB Flash图片和PCB Flash煅烧。TGA曲线表明，PCB飞边在约400°C时开始减重，在约800°C时保持稳定。(C)PCB的TGA曲线。(d)PCB、PCB闪光和PCB闪光煅烧的X射线光电子能谱(XPS)。PCB的XPS主要显示C和一些无机信号。PCB闪光的XPS大多显示C信号，表明O在FJH过程中被去除，没有检测到无机元素峰，可能是因为在FJH过程中无机物被碳覆盖。PCB快速煅烧的XPS显示出丰富的元素信号，表明无机材料的去除和暴露。(e)PCB中贵金属的浓度-煅烧。(f)通过煅烧提高浸出率。Y0和Y分别表示PCB浸出和PCB煅烧的回收率。

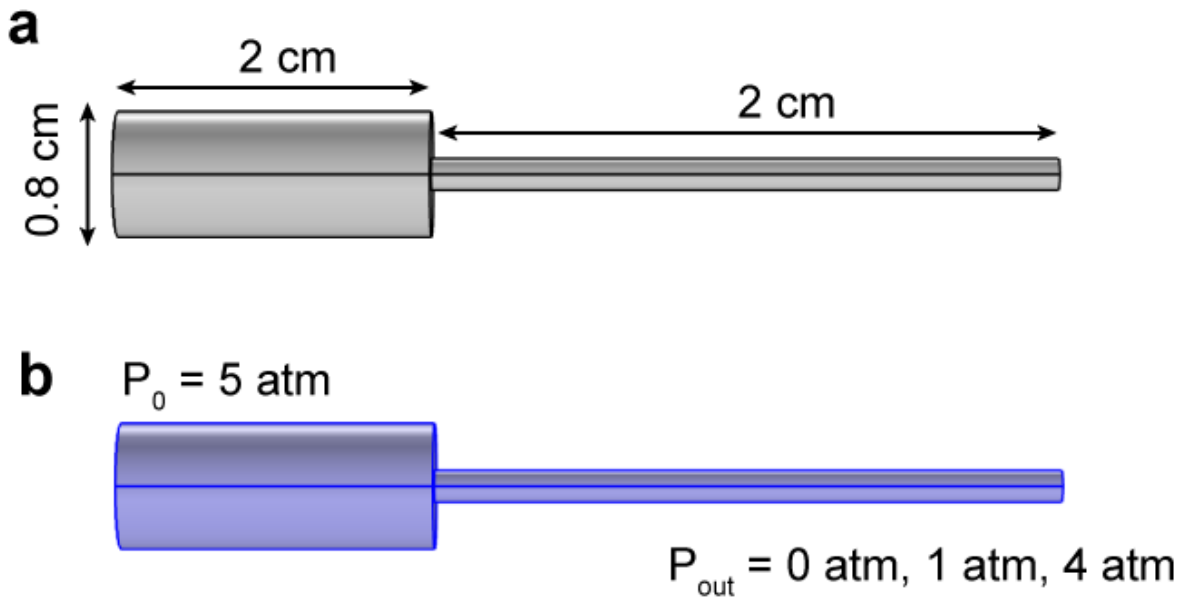

补充图18 |气流模拟。（a）几何条件。（b）边界条件

Supplementary Fig. 18 | Gas flow simulation. (a) Geometrical conditions. (b) Boundary conditions.

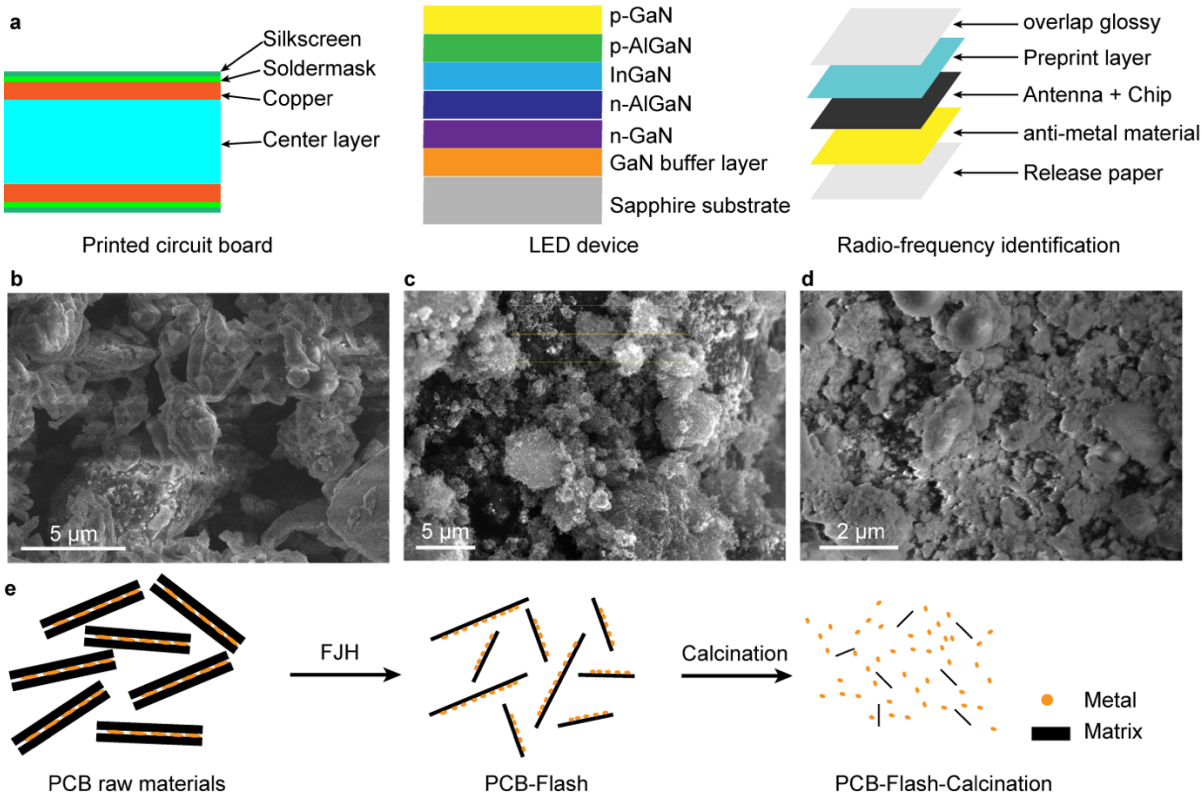

补充图19 |闪蒸提高浸出效率的机理

Supplementary Fig. 19 | Mechanism of the improvement of leaching efficiency by flash Joule heating (FJH). (a) Scheme of the laminated configuration of several types of electronics. (b) Scanning electron microscopy (SEM) image of printed circuit board (PCB) powders. (c) SEM image of PCB-Flash. (d) SEM image of PCB-Flash-Calcination. (e) The scheme of morphological and structure changes of PCB during the FJH and calcination process.

焦耳加热(FJH)。(a)几种类型电子器件的层压配置方案。(b)印刷电路板(PCB)粉末的扫描电子显微镜(SEM)图像。(c)PCB闪光的SEM图像。(d)PCB快速煅烧的SEM图像。(e)介绍了PCB在FJH和煅烧过程中的形态和结构变化方案。

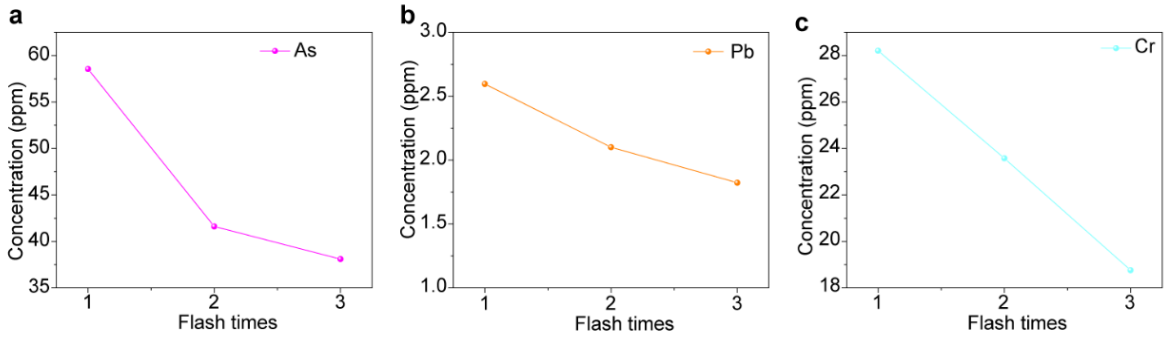

补充图20 |多次闪蒸后剩余重金属浓度

Supplementary Fig. 20 | Concentration of remaining heavy metals after multiple flash 焦耳加热(FJH)反应。(a)砷的浓度。(b)铅的浓度。(c)铬的浓度。每个FJH为1s。

Joule heating (FJH) reactions. (a) Concentration of As. (b) Concentration of Pb. (c) Concentration of Cr. Each FJH is 1 s.

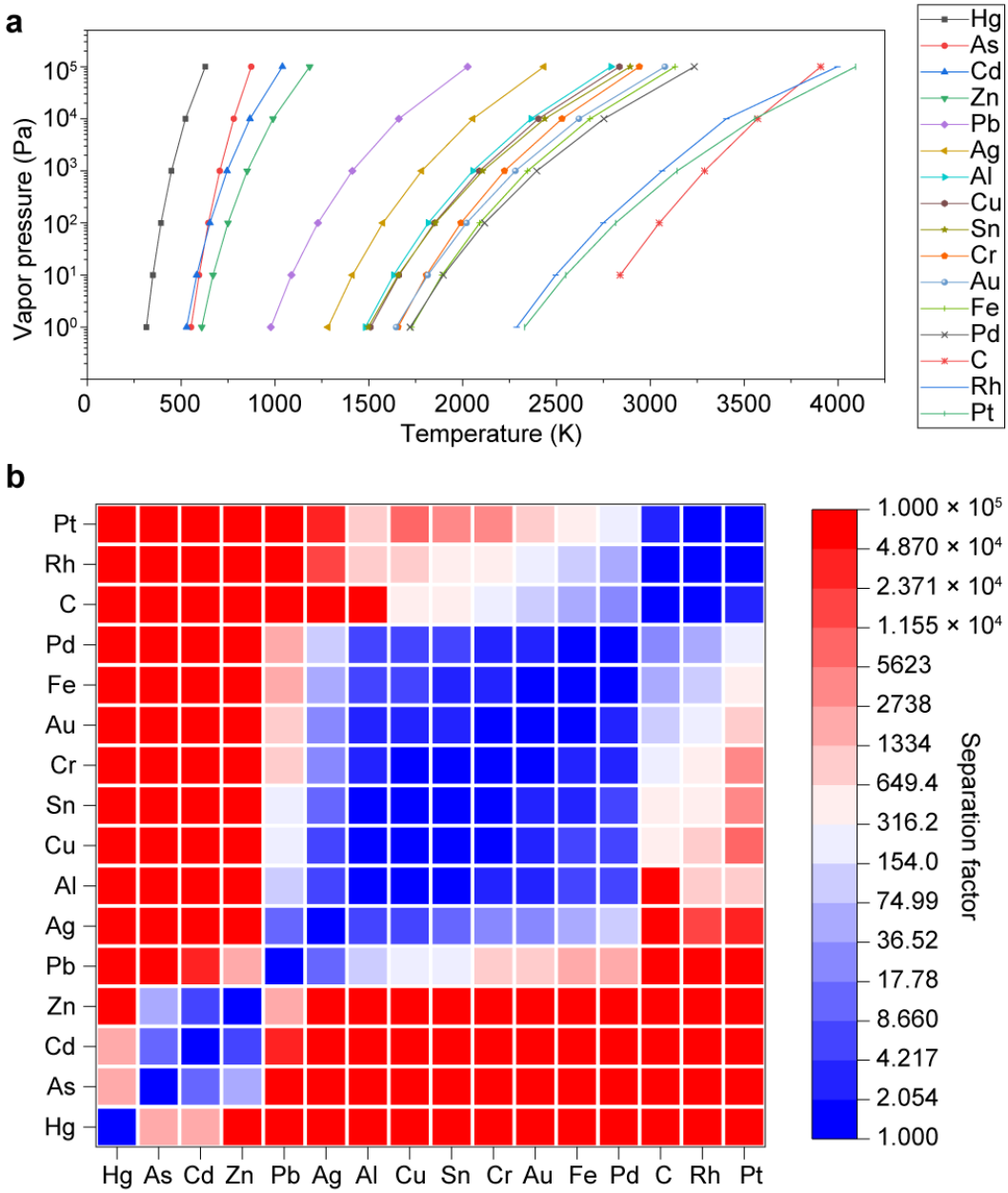

补充图21。蒸发分离的理论分离系数

Supplementary Fig. 21. Theoretical separation factor of the evaporative separation process. (a) Vapor pressure-temperature relationship of 16 representative elements. (b) Heatmap of the theoretical separation factors for the 16 elements.

(a) 16种代表性元素的蒸气压-温度关系。(b) 16种元素的理论分离系数热图。

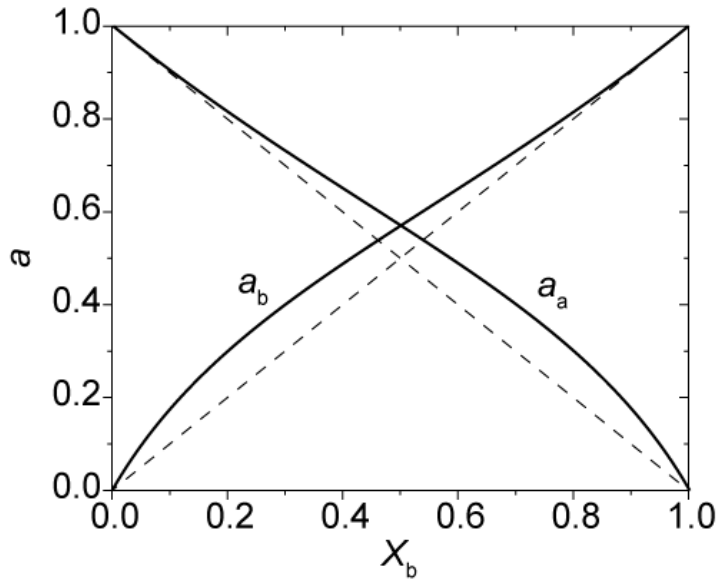

补充图22。活动组成关系。

Supplementary Fig. 22. Activity-composition relationship.

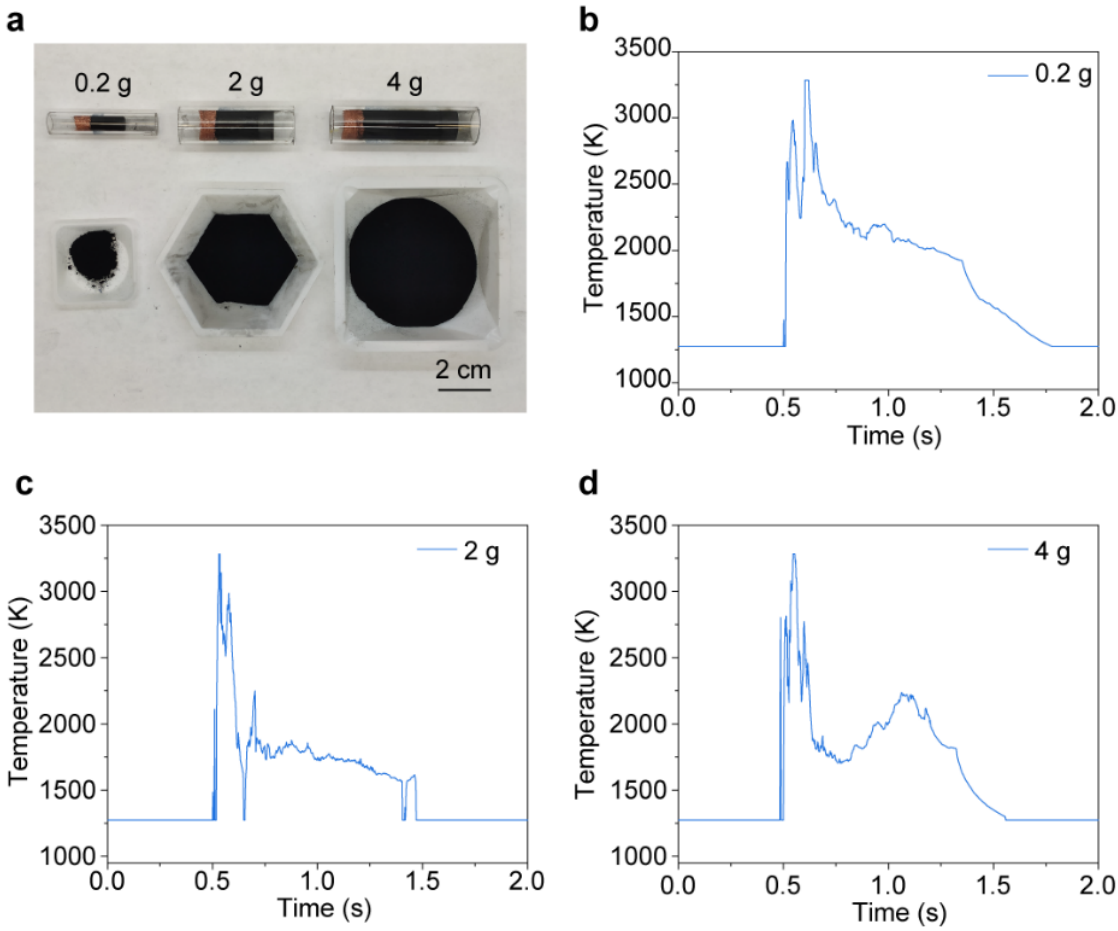

补充图23。闪光焦耳加热(FJH)工艺的放大。(a)的图片

Supplementary Fig. 23. Scaling up of the flash Joule heating (FJH) process. (a) Picture of

在m0=0.2 g、V0=150 V和C0=0.06 F(左)、m1=2 g、V1=150 V和C1=0.6 F(中)、m2=4 g、

the samples treated with the condition of m_0 = 0.2 g, V_0 = 150 V, and C_0 = 0.06 F (left), m_1 = 2

V2=300 V和C2=0.6 F(右)的条件下处理的样品。(b-d

g, V_1 = 150 V, and C_1 = 0.6 F (middle), m_2 = 4 g, V_2 = 300 V, and C_2 = 0.6 F (right). (b-d)

)质量为m0=0.2 g(b)，m1=2 g(c)，m2=4 g(d)的样品的实时温度曲线。

Realtime temperature curves for samples with mass of m_0 = 0.2 g (b), m_1 = 2 g (c), and m_2 = 4

g (d).

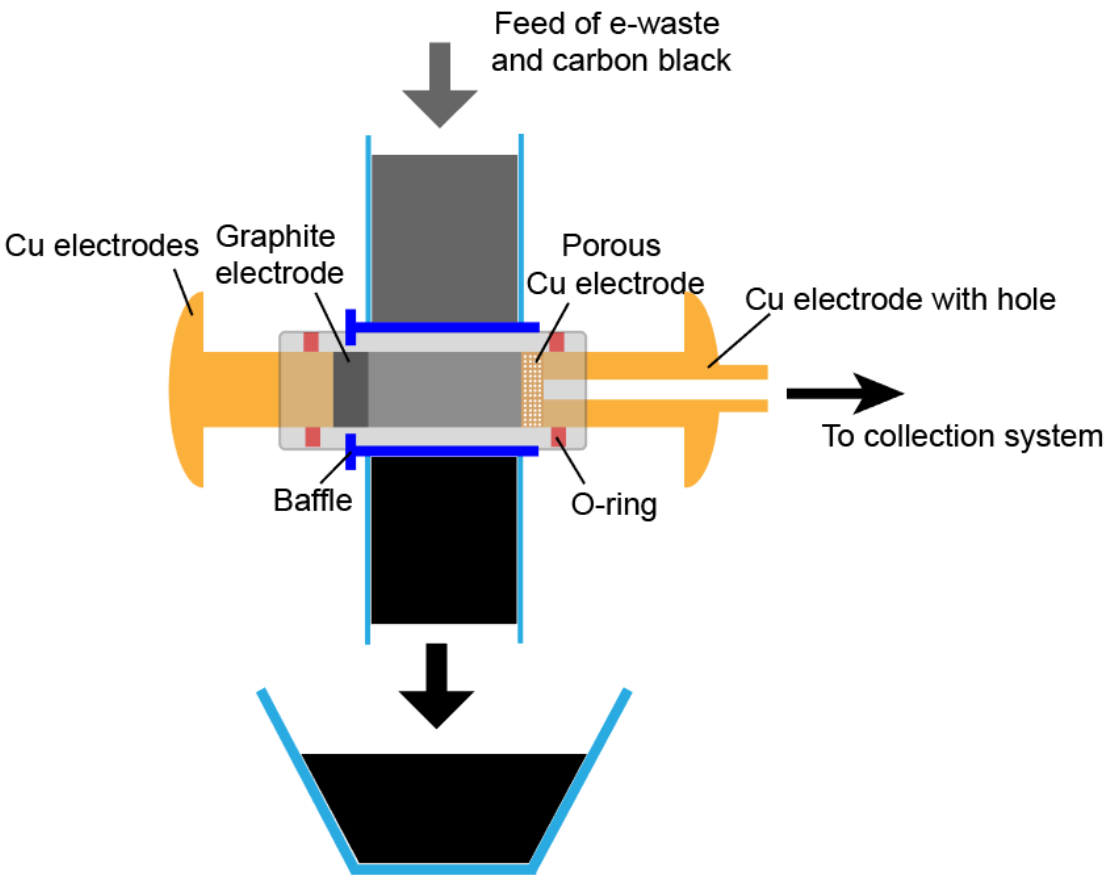

补充图24。 电子废物处理用连续闪速焦耳加热(FJH)反应器的方案。

Supplementary Fig. 24. The scheme of a continuous flash Joule heating (FJH) reactor for e-waste processing.

补充表1。真空下FJH的参数。

Supplementary Table 1. Parameters for FJH under vacuum.

前体 Precursors	质量比 Mass Ratio	质量(mg) Mass (mg)	电阻( ) Resistance (Ω)	电压(V) Voltage (V)	时间(s) Time (s)
PCB:CB, 1#	2:1	300	1.8	150	1
PCB:CB, 2#	2:1	300	2.0	150	1
PCB:CB, 3#	2:1	300	2.5	150	1
PCB:CB:NaCl, 1#	1:2:3	300	2.3	150	1
PCB:CB:NaCl, 2#	1:2:3	300	1.9	150	1
PCB:CB:NaCl, 3#	1:2:3	300	1.8	150	1
PCB:CB:KCl, 1#	1:2:3	300	22	150	1
PCB:CB:KCl, 2#	1:2:3	300	18	150	1
PCB:CB:KCl, 3#	1:2:3	300	14	150	1
PCB:CB:PVC, 1#	1:2:3	300	2.0	150	1
PCB:CB:PVC, 2#	1:2:3	300	2.5	150	1
PCB:CB:PVC, 3#	1:2:3	300	2.5	150	1
PCB:CB:CPVC, 1#	1:2:3	200	3.0	150	1
PCB:CB:CPVC, 2#	1:2:3	200	3.0	150	1
PCB:CB:CPVC, 3#	1:2:3	200	3.2	150	1
PCB:CB:NaF, 1#	1:2:3	200	1.5	150	1
PCB:CB:NaF, 2#	1:2:3	200	1.0	150	1
PCB:CB:NaF, 3#	1:2:3	200	1.0	150	1
PCB:CB:PTFE, 1#	1:2:3	200	2.0	150	1
PCB:CB:PTFE, 2#	1:2:3	200	2.2	150	1
PCB:CB:PTFE, 3#	1:2:3	200	2.2	150	1
PCB:CB:NaI, 1#	1:2:3	200	0.6	150	1
PCB:CB:NaI, 2#	1:2:3	200	0.6	150	1
PCB:CB:NaI, 3#	1:2:3	200	0.5	150	1
PCB:CB:NaF:NaCl:NaI, 1#	1:2:1:1:1	200	0.2	150	1
PCB:CB:NaF:NaCl:NaI, 2#	1:2:1:1:1	200	1	150	1
PCB:CB:NaF:NaCl:NaI, 3#	1:2:1:1:1	200	0.5	150	1

补充表2。压力下FJH的参数。

Supplementary Table 2. Parameters for FJH under pressure.

前体 Precursors	质量比 Mass Ratio	大量 Mass (mg)	反对 Resistance (Ω)	压力 Pressure	电压 Voltage (V)	时间 Time (s)	FJH后的质量 Mass after FJH (mg)
PCB:CB	2:1	200	1.0	1巴10 1 bar	10	1	196
PCB:CB	2:1	200	1.3	1巴30 1 bar	30	1	196
PCB:CB	2:1	200	1.0	1巴50 1 bar	50	1	180
PCB:CB	2:1	200	1.0	1巴100 1 bar	100	1	158
PCB:CB	2:1	200	1.0	1巴120 1 bar	120	1	115
PCB:CB	2:1	200	1.0	真空120 vacuum	120	1	65
PCB:CB	2:1	200	1.0	1巴120 1 bar	120	1	115
PCB:CB	2:1	200	1.0	2巴120 2 bar	120	1	142
PCB:CB	2:1	200	1.0	3巴120 3 bar	120	1	155
PCB:CB	2:1	200	1.0	4巴120 4 bar	120	1	165

Supplementary Table 3. The calculated separator factor of the evaporative separation process.

	Hg	As	Cd	Zn	Pb	Ag	Al	Cu	Sn	Cr	Au	Fe	Pd	C	Rh	Pt
Hg	1	2309	2309	50000	100000	100000	100000	100000	100000	100000	100000	100000	100000	100000	100000	100000
As	2309	1	9.13	69.9	100000	100000	100000	100000	100000	100000	100000	100000	100000	100000	100000	100000
Cd	2309	9.13	1	5.71	28089	100000	100000	100000	100000	100000	100000	100000	100000	100000	100000	100000
Zn	50000	69.9	5.71	1	2066	100000	100000	100000	100000	100000	100000	100000	100000	100000	100000	100000
Pb	100000	100000	28089	2066	1	12.1	129	175	206	680	913	1961	2439	100000	100000	100000
Ag	100000	100000	100000	100000	12.1	1	6.69	8.64	10	19.8	35	56.1	78.7	100000	19083	34130
Al	100000	100000	100000	100000	129	6.69	1	1.25	1.65	2.31	4.21	5.5	8.32	100000	735	1235
Cu	100000	100000	100000	100000	175	8.64	1.25	1	1.3	1.8	3.35	4.43	6.5	513	870	10000
Sn	100000	100000	100000	100000	206	10	1.65	1.3	1	1.3	2.45	3.39	5.19	349	584	5618
Cr	100000	100000	100000	100000	680	19.8	2.31	1.8	1.3	1	1.96	2.57	3.89	247	401	3141
Au	100000	100000	100000	100000	913	35	4.21	3.35	2.45	1.96	1	1.28	2.16	90.6	160	754
Fe	100000	100000	100000	100000	1961	56.1	5.5	4.43	3.39	2.57	1.28	1	1.59	61.1	105	443
Pd	100000	100000	100000	100000	2439	78.7	8.32	6.5	5.19	3.89	2.16	1.59	1	31.7	60.2	172
C	100000	100000	100000	100000	100000	100000	100000	513	349	247	90.6	61.1	31.7	1	1.4	2.18
Rh	100000	100000	100000	100000	100000	19083	735	870	584	401	160	105	60.2	1.4	1	1.48
Pt	100000	100000	100000	100000	100000	34130	1235	10000	5618	3141	754	443	172	2.18	1.48	1

Note: The theoretical separation factors are calculated based on the vapor pressure difference of pure metals. They represent practical values for trace metals separation from abundant metals. For the separation of abundant metals, the values should be corrected according to their activity in the alloy melt.

补充表4。 贵金属的分离因子。

Supplementary Table 4. The separation factors of precious metals.

	Rh	Pd	Ag	Au
Rh	1	1.29	9.5	3.1
Pd	1.29	1	12.3	2.4
Ag	9.5	12.3	1	29.2
Au	3.1	2.4	29.2	1

补充表5。 NaCl添加剂分离贵金属的影响因素

Supplementary Table 5. The separation factors of precious metals by using NaCl additives

	Rh	Pd	Ag	Au
Rh	1	1.44	3.0	840
Pd	1.44	1	4.33	58.3
Ag	3.0	4.33	1	253
Au	840	58.3	253	1

补充表6。 NaF添加剂分离贵金属的影响因素

Supplementary Table 6. The separation factors of precious metals by using NaF additives

	Rh	Pd	Ag	Au
Rh	1	1.52	1.8	146
Pd	1.52	1	1.19	96
Ag	1.8	1.19	1	81
Au	146	96	81	1

补充表7。 NaI添加剂分离贵金属的影响因素

Supplementary Table 7. The separation factors of precious metals by using NaI additives

	Rh	Pd	Ag	Au
Rh	1	1.05	1.08	1.59
Pd	1.05	1	1.03	1.51
Ag	1.08	1.03	1	1.48
Au	1.59	1.51	1.48	1

补充表8。ICP-MS标准。

Supplementary Table 8. Standards for ICP-MS.

标准 **Standards**	元素 **Elements**	浓度矩阵 **Concentrations**	**Matrix**
元素周期表混合物1 Al、As、Ba、Be、Bi、B、Ca、Cd、Cs、Cr、Co、 Periodic table mix 1	Al, As, Ba, Be, Bi, B, Ca, Cd, Cs, Cu、Ga、In、Fe、Pb、Li、Mg、Mn、Ni Cr, Co, Cu, Ga, In, Fe, Pb, Li, Mg, 、P、K、Rb、Se、Si、Ag、Na、Sr、S、 Mn, Ni, P, K, Rb, Se, Si, Ag, Na, Te、Tl、V和Zn Sr, S, Te, Tl, V, and Zn	10毫克/升 10 mg/L	10% HNO_3
元素周期表混合物2 Au、Ge、Hf、Ir、Mo、Nb、Pd、Pt、Re、Rh、Ru、 Periodic table mix 2	Au, Ge, Hf, Ir, Mo, Nb, Pd, Pt, Re, Sb、Sn、Ta、Ti、W和Zr Rh, Ru, Sb, Sn, Ta, Ti, W, and Zr	10毫克/升 10 mg/L	5% HCl, 1% HF
元素周期表混合物3 Sc、Y、La、Ce、Pr、Nd、Sm、Eu、Gd、Tb、Dy、 Periodic table mix 3	Sc, Y, La, Ce, Pr, Nd, Sm, Eu, Gd, Ho、Er、Tm、Yb和Lu Tb, Dy, Ho, Er, Tm, Yb and Lu	10毫克/升 10 mg/L	5% HNO_3
水星 Mercury	Hg	1000毫克/升 1000 mg/L	12% HNO_3

补充参考文献

Supplementary References

1 Bernardis，F.L.，Grant，R.A.和Sherrington，D.C。铂族金属氯络合物分离方法综述。反应 功能。Polym公司。65, 205-217 (2005).

1 Bernardis, F. L., Grant, R. A. & Sherrington, D. C. A review of methods of separation of the platinum-group metals through their chloro-complexes. *React. Funct. Polym.* **65**, 205-217 (2005).

2 Ueda，T.、Ichishi，S.、Okuda，A.和Matsutani，K.《金属可持续性：全球挑战、后果和前景》(ed Reed M.Izatt)333-360(John Wiley&Sons，Ltd，2016)。

2 Ueda, T., Ichiishi, S., Okuda, A. & Matsutani, K. in *Metal Sustainability: Global Challenges, Consequences, and Prospects* (ed Reed M. Izatt) 333-360 (John Wiley & Sons, Ltd, 2016).

3 Yousif，A.M.使用湿法冶金技术和连续沉淀法从废汽车催化转化器中回收并单独分离铂、钯和铑。J. 化学。2019 (2019).

3 Yousif, A. M. Recovery and Then Individual Separation of Platinum, Palladium, and Rhodium from Spent Car Catalytic Converters Using Hydrometallurgical Technique followed by Successive Precipitation Methods. *J. Chem.* **2019** (2019).

4 Charlesworth，P.通过液-液萃取分离铂族金属。白金金属漆。 修订版。25, 106-112 (1981).

4 Charlesworth, P. Separating the platinum group metals by liquid-liquid extraction. *Platinum Met. Rev.* **25**, 106-112 (1981).

5 2000年以后的金属分离技术：将新化学与加工相结合，研讨会论文集，夏威夷，6月13日至18日，TMS，1999年，第357-370页。

5 Metal Separation Technologies beyond 2000: Integrating Novel Chemistry with Processing, Symposium Proceeding, Hawaii, June 13-18, TMS, 1999, pp. 357-370.

6 Dong，Z.H.等人。镍基合金中镍、铝和铬的蒸发及其对单晶组件制造过程中表面缺陷形成的影响。金属材料。 变速箱。

6 Dong, Z. H. *et al.* Vaporization of Ni, Al and Cr in Ni-Base Alloys and Its Influence on Surface Defect Formation During Manufacturing of Single-Crystal Components. *Metall Mater. Trans. A* **51**, 309-322 (2020).

7 Balaji，R.&Senophiyah Mary，J.，《城市采矿和可持续废物管理》(ed Sadhan Kumar Ghosh)59-67(Springer Singapore，2020)。

7 Balaji, R. & Senophiyah-Mary, J. in *Urban Mining and Sustainable Waste Management* (ed Sadhan Kumar Ghosh) 59-67 (Springer Singapore, 2020).

8 Theo，L.《1998年IEEE电子与环境国际研讨会论文集》。ISEE-1998(目录。

8 Theo, L. in *Proceedings of the 1998 IEEE International Symposium on Electronics and the Environment. ISEE - 1998 (Cat. No.98CH36145).* 42-47.

9 Luong，D.X.等人，《克级自下而上快速石墨烯合成》。《自然》577647-651(2020)。

9 Luong, D. X. *et al.* Gram-scale bottom-up flash graphene synthesis. *Nature* **577**, 647-651 (2020).

10 Stanford，M.G.等人，《闪光石墨烯形态》。ACS Nano 14，13691-13699(2020年)。

10 Stanford, M. G. *et al.* Flash Graphene Morphologies. *ACS Nano* **14**, 13691-13699 (2020).

11 Algozeeb，W.A.等人从塑料废料中提取石墨烯。 ACS Nano 14，15595-15604(
11 Algozeeb, W. A. *et al.* Flash graphene from plastic waste. *ACS Nano* **14**, 15595-15604
2020年)。
(2020).

12 Okamoto，H.，Schlesinger，M.E.，Mueller，E.M.，ASM手册第3卷：合金相图，(ASM
12 Okamoto, H., Schlesinger, M. E., Mueller, E. M., ASM Handbook Volume 3: Alloy
International，俄亥俄州，2016)
Phase Diagrams, (ASM International, Ohio, 2016)

13 CRC化学和物理手册。 互联网版本2005 edn(CRC出版社，2005年)
13 *CRC Handbook of Chemistry and Physics*. Internet Version 2005 edn, (CRC Press,
。
2005).

14 Jayne，D.T.，Fatemi，N.S.和Weizer，V.G。 Auxin合金的X射线光电子能谱研究。
14 Jayne, D. T., Fatemi, N. S. & Weizer, V. G. An X-Ray Photoelectron-Spectroscopy
J. 真空吸尘器技术。
Study of Auxiny Alloys. *J. Vac. Sci. Technol. A* **9**, 1410-1415 (1991).

15 Andersson，S.L.T.，Watters，K.L.和Howe，R.F。 Rh6(Co)16-Al2O3的XPS研究。J. 加
15 Andersson, S. L. T., Watters, K. L. & Howe, R. F. An XPS Study of $Rh_6(Co)_{16}$-Al_2O_3.
泰罗尼亚。
J. Catal. **69**, 212-215 (1981).

16 Sleigh，C.、Pijpers，A.P.、Jaspers，A.、Coussens，B.和Meier，R.J。 通过ESCA测定原子电荷，
16 Sleigh, C., Pijpers, A. P., Jaspers, A., Coussens, B. & Meier, R. J. On the determination
包括对有机金属的应用。 J. 电子光谱
of atomic charge via ESCA including application to organometallics. *J. Electron*
。
Spectrosc. **77**, 41-57 (1996).